Fair-Weather Cumulus Clouds Forming over the Urban Area in Northern Tokyo

January 2008

Tadao INOUE

Fair-Weather Cumulus Clouds Forming over the Urban Area in Northern Tokyo

A Dissertation Submitted to
the Graduate School of Life and Environmental Sciences,
the University of Tsukuba
in Partial Fulfillment of the Requirements
for the Degree of Doctor of Philosophy in Science
(Doctoral Program in Geoenvironmental Sciences)

Tadao INOUE

Abstract

The urban effects on cumulus clouds and their forming mechanisms in northern Tokyo are investigated by a satellite image analysis, a photographic observation, and numerical experiments in this study.

The frequency distribution of low-level clouds that are expected to be shallow cumulus clouds is estimated around the Tokyo metropolitan area in summer without regional-scale cloud cover using NOAA satellite images during an 11-year period. The urban area is determined by the Normalized Difference Vegetation Index (NDVI) obtained by the same satellite. The low-level cloud frequency is higher over this large urban area than over rural areas in the early afternoon, especially over the radially extending urban areas along major railroads from Tokyo. We can conclude that the frequency of the low-level clouds is enhanced over the urban area, since the cloud frequency is negatively well correlated with the NDVI and their peaks fit well within a shift of about 2 km. The frequency of low-level clouds, however, is quite low in the coastal zone, even in the urban area, because of sea breezes.

To investigate the features of the urban clouds, the ground-based photographic observation was conducted around Saitama City in northern Tokyo, where the contrast of cloud frequency between urban and rural areas is sharp. The urban clouds were observed on 12 days in 54 days when photographs were taken. The horizontal cloud distribution was confirmed by the images of the Moderate Resolution Imaging Spectroradiometer (MODIS) aboard the Terra and Aqua satellites. The urban clouds formed cloud lines along the urban area. In the most case, the onset time of the urban clouds was between 0800 LST and 1130 LST, and the dissipation time was between 1300 LST and 1700 LST, although the time evolution of clouds somewhat depended on days. The duration of the cloud forming ranged between 3 to 6 hours in the most days. Those

clouds were generally active cumulus clouds, whose tops penetrated into the level of free convection. The clouds were gradually developed and became cumulus congestus in the early afternoon on some of those days.

The cloud lines along the urban areas are simulated by a numerical model with a simplified urban surface parameterization. Horizontal distribution of the simulated clouds agrees well with the observed clouds in satellite images. Some sensitivity tests indicate that the urban thermal effect enhances cloud formation, but it suppresses clouds in the adjacent rural areas. The distribution of the simulated clouds agrees well with the observations, when the maximum sensible heat flux in the urban area is about seven times larger than that in the rural areas. With reduction of the thermal contrast, the cloud suppression in the rural areas is gradually weakened. The contrast of cloud distribution is still clear even when the ratio of sensible heat fluxes between urban and rural is 4.3, but it becomes unclear when the ratio is 1.9. The mechanisms of the cloud contrast are as follows: 1) Thermals form in the mixed layer above the land surface. 2) Because of larger sensible heat flux, the mixed layer tends to be higher in the urban areas so that thermals are easier to reach the lifting condensation level than the rural areas. 3) Wide compensating downdrafts of the strong urban thermals cover the entire rural areas and suppress thermals and clouds there.

Key words: cumulus cloud, satellite, photographic observation, numerical model, thermal, urban heat island, sensible heat flux

Contents

List of figures

List of Tables

1. Introduction

A prominent clear heat island has been reported around the Tokyo, one of the largest metropolitan areas in the world. The urban area may affect not only the surface temperature but also the clouds and precipitation. On the other hand, local heavy rains in urban areas have become one of the social problems in many cities, especially in the big cities. Although the urban effects on local heavy rains have been indicated in many studies, the mechanisms of them still are not clarified. Convective clouds like cumulus clouds have a close relation to local heavy rains, but only a few studies have investigated the effects of urbanization on clouds.

1.1. Urban effects on precipitation

A large field project, METROMEX, was conducted to study inadvertent weather modifications resulting from urban and industrial effects in the St. Louis area, in a relatively flat area in Missouri and Illinois, U.S.A. (Changnon et al., 1971). Changnon et al. (1976) and Changnon (1978) showed statistically significant increases in summer rainfall in and around St. Louis. Braham and Wilson (1978) showed an enhancement in the frequency of tall echoes of radar over the city and near-downwind areas. Recently, Bornstein and Lin (2000) analyzed surface meteorological network data around Atlanta and pointed out that the urban heat island induces a convergence zone and often initiates storms. Shepherd et al. (2002) showed that the Precipitation Radar on board tropical rainfall measuring mission (TRMM/PR) could be used to identify urban-induced rainfall anomalies. The trend of increasing heavy rain in Tokyo was indicated by some statistic studies (Yonetani, 1982; Fujibe, 1998; Sato and Takahashi, 2000). By using long-term radar echo data, Sato et al. (2006) indicated that the frequency of precipitation in

the urban area is higher than surrounding areas when the precipitation system moves from mountain areas to the plain. They implied that the urban area reinforces the moving precipitation systems.

Although many studies suggested that anthropogenic effects are likely to induce or reinforce precipitation around urban areas, the underlying mechanisms have remained unclear (Shepherd, 2005). One of the major difficulties in investigating the urban-induced precipitation is that convective rain may occur anywhere with a small trigger in case of unstable atmospheric conditions (Fujibe, 2004). Another difficulty is that convective rain tends to occur occasionally and often disappear chaotically. Since variations of precipitation events usually are quite different each other, the process of the urban-induced precipitation is difficult to generalize from a limited observation data. Furthermore the urban effects are usually much weaker than the topographic effects induced by surrounding mountains or the land/sea contrast.

1.2. Urban effects on cloud

Obviously, clouds are forming much more frequently than the deep convection over the land surface and may be more easily affected by the anthropogenic surface conditions. Difference in cloud frequency between urban and rural should provide information on the mechanism of the urban-induced precipitation.

Ochs (1975) conducted two-dimensional numerical experiments and suggested that high surface air temperature can be a cause of initiation and development of cumulus. Grosh (1978) studied the relationship between precipitation and the frequency distribution of cloud around St. Louis urban area. In the last decade, some statistical studies showed that clouds tend to form in an urban area more than surrounding areas using satellite data. Rabin and Martin (1996) investigated the cloud frequency in dry and wet summers over the central United States and indicated that the cloud frequency is high in some of urban areas. Romanov (1999) compared the

ratio of cloud cover and the clear-sky frequency over the high-rise area of downtown Moscow and its suburbs using three-year NOAA satellite images. He pointed out that there was an increase in the cloud cover over most of the city area during the warm periods of spring and summer.

Baik et al. (2001) investigated dry and moist convection forced by an urban heat island using a two dimensional numerical model. They concluded that updraft cells induced by the urban heat island can initiate moist convection. Using a three dimensional high-resolution numerical model, Kanda et al. (2001) recreated a small cloud line, which can be sometimes observed near Tokyo. Their numerical experiments indicated that the cloud line forms above the convergence line between two sea breezes near Tokyo. They also suggested that the past sprawling of Tokyo may have changed the intensity and the position of the cloud line. This fact implies that the actually observable cloud system may be formed by the urban effects.

Besides the urban effects, more general land surface effects on the fair-weather clouds have been well investigated. Using a two dimensional high-resolution mesoscale model, Chen and Avissar (1994) showed that land surface moisture significantly affects the timing of onset of clouds and the intensity of precipitation. Avissar and Liu (1996) conducted a three-dimensional numerical study on similar topics and stated that clouds and precipitation are strongly affected by landscape structure. When land surface is homogeneous, shallow convective clouds are distributed randomly. On the other hand, when land surface moisture is heterogeneous, the land surface structure triggers the formation of mesoscale circulations, and then clouds concentrate in the dry part of the domain. Since precipitation becomes larger in the dry part, this process creates a negative feedback, which tends to eliminate the discontinuities of land surface moisture and spatially homogenize the land water content.

1.3. Urban effects on wind field

The urban area also affects the regional scale wind field on calm days. Shreffler (1978) showed statistically that the convergence toward St. Louis urban area is stronger in daytime than in nighttime. Fujibe and Asai (1980) also indicated that the existence of week convergence toward the center of Tokyo in daytime of calm summer days statistically. They implied that the convergence is induced by the updraft of urban areas. Furthermore, Yoshikado and Kondo (1989) and Yoshikado (1990) indicated that the inland penetration of sea breeze is affected by a heat island of the coastal urban area.

Kimura and Takahashi (1991) simulated the urban heat island of the Tokyo metropolitan area. They indicated that convergence exists northwest of center of Tokyo, and it was formed by urban heat island of Tokyo. Kusaka et al. (2000) simulated the changes of a sea breeze and the urban heat island due to the 85-year land use alternation. They suggested that the urban effects enhance horizontal convergence around the urban area. Fujibe (2003) supported the idea by the statistic study of long-term wind observation data.

1.4. Vertical structure of urban mixed layer

The higher surface air temperature in urban areas may affect the structure of boundary layer. Hjelmfelt (1982) simulated the urban and rural boundary layers around St. Louis by using three-dimentional numerical model. He implied that the upward air motion occurred downwind of the city primarily as a result of the urban effect. Hildebrand and Ackerman (1984) showed that the vertical turbulent intensities are enhanced in the urban area, in addition, the height of the urban boundary layer is higher than the rural one by using instrumented aircraft. Kusaka et al. (2000) showed by numerical simulations that higher sensible heat flux from larger urban area increases the cumulative heat in an atmospheric column.

1.5. Aerosol effect on urban cloud and precipitation

Cloud formation may be also affected by cloud condensation nuclei (CCN) emitted from the urban area. Ochs and Semonin (1979) employed a parcel model of condensation and suggested that the observed differences in the first echo between urban and rural clouds do not result from the concentration differences in any CCN size range. Later studies by Frisbie and Hudson (1993) could not provide a strong evidence of cloud formation by the urban CCN. Furthermore, Jin et al. (2005) indicated that the anthropogenic-induced weekly cycles of aerosols and clouds are weak.

1.6. Purpose of the study

The purpose of the study is to clarify the urban effect on cumulus clouds and their forming mechanisms in the northern part of the Tokyo metropolitan area. First, the urban effects on the frequency distribution of shallow clouds around Tokyo in summer are investigated by using long-term satellite images. Second, to find the features of the urban clouds, the ground-based photographic observation was conducted. Third, the small cloud lines above the urban areas are simulated by using a three-dimensional mesoscale numerical model, and sensitivity experiments are also conducted focused on the thermal contrast between urban and rural areas. Finally, the mechanisms of the cloud formation in urban areas and cloud suppression in the adjacent rural areas will be discussed.

2. Distribution of shallow clouds frequency in summer around large urban area

2.1. Data and Methods

Low-level clouds were detected using 11-year data of the Advanced Very High Resolution Radiometer (AVHRR) aboard satellite NOAA, which are received and archived by the Center for Northeast Asian Studies of Tohoku University, Japan. The spatial resolution of an original image is about 1.1 km. Each image covers eastern Japan, which includes the Kanto Plain, and consists of 1024×1024 pixels after being converted into a map of the Mercator projection. The AVHRR data were recorded once a day and observed in the early afternoon, mostly from 1200 to 1500 LST (0300 to 0600 UTC). The intensity of each channel was classified into 256 levels. The location, topography, and land uses of the analyzing domain is shown in Figures 2.1a-c, respectively.

The Kanto Plain extends over an area of about 120×120 km. The western and northern parts of the plain are surrounded by mountains with a height of more than 1000 m (see Figure 2.1b). In the figure, squares and stars indicate the location of the Automated Meteorological Data Acquisition System (AMeDAS) surface observation stations operated by the Japan Meteorological Agency (JMA). The stations indicated by stars will be referred to in the following sections, and their names are abbreviated as follows; To: Tokyo; Ne: Nerima; Ur: Urawa (The name of this station is changed to “Saitama” after Section 3); Ch: Chiba; Mi: Mito; Ut: Utsunomiya; Ma: Maebashi; Ku: Kumagaya; Ab: Abiko; Ry: Ryugasaki; Ha: Hachiouji; and Yo: Yokohama. The shaded areas indicate water surface. The study period included the months of July and August in 1990 to 2000.

Image data were rejected from the statistical analysis when clouds covered the entire study

area or the receiving conditions were poor. In the present paper, "clear day" means that the land surface over 10% of the Kanto Plain could be observed in the AVHRR images. As a result, 328 "clear days" were selected from a total of 682 days in July-August during an 11-year period (hereafter referred to as "the selected days").

We focus the following discussions on low-level clouds that are expected to be shallow cumulus clouds and should be more sensitive to the ground surface conditions than higher clouds. The frequency distribution of low-level clouds was estimated by the following three steps. In the first step, clouds were detected by the difference in albedo observed by channel 1 of the AVHRR data. The threshold of the brightness level was assumed to be 100 in 256 classified levels; this is a slightly higher brightness level than the highest ground surface reflectance.

The second step is to remove high-level clouds. High-level clouds often appeared in the study area and weakened the signals of low-level clouds. We assumed a threshold of brightness temperature of 282 K that roughly corresponded to the atmospheric temperature at a level about 3200 m above sea level. It can remove deep convection over the Plain. Although some of deep convection may be induced by the urban effect, we neglect them because we focus only on the low-level clouds.

If a pixel met the two requirements above, we assume that the pixel indicated a low-level cloud; then, the pixel is designated as "1;" otherwise, it was designated as "0." Figures 2.2a and 2.2b show a sample of the images of channel 1 with 256 levels and the same image by the two values (0 or 1), respectively.

The third step is the summation of the two values in the selected 328 images for each pixel. The frequency distribution is obtained by the average in 2×2 pixels and will be referred to as the "grid" hereafter.

The urban areas are defined by the Normalized Difference Vegetation Index (NDVI), since urbanized areas are covered by less vegetation in the Tokyo metropolitan area. The composite NDVI image consists of the maximum value of each pixel obtained in July-August 1991 (21

days).

2.2. Results

Figure 2.3a shows the composite NDVI during summer in 1991 in the area en-closed by the broken lines in Figure 2.1. The stars in Figures 2.3 indicate the observation stations that are also shown in Figure 2.1 with abbreviated station names. The lower NDVI areas (the dark areas in Figure 2.3a) are expected to be highly urbanized areas or water surface. The major urban area extends toward the inland area up to a radius of 20 km from the center of Tokyo, located near the coastline of the Tokyo Bay (hereafter, this area will be referred to as "the major urban area"). Most of the major urban area is the Tokyo metropolis. The observation station labeled "To" is located in one of the major business centers in Tokyo.

Some arm-like urban areas extend along the major highways or railroads from the major urban area of Tokyo (hereafter referred to as "the radial urban areas"); therefore, the entire urban area assumes the shape of a starfish. The ellipses drawn by broken lines in Figures 2.3a and 2.3b indicate some typical radial urban areas that we focus on. The high-NDVI areas in the western and northwestern parts of the domain correspond to the mountainous areas. The dark shaded area around 36.0°N and 140.4°E is Lake Kasumigaura.

Figure 2.3b shows the low-level cloud frequency in summer during the 11-year period. The lighter shades indicate a higher cloud frequency. The low-level cloud frequency is the highest in the mountainous areas, and the second highest frequency appears in the plain followed by that in the coastal areas. The maximum value in the domain is 47%, observed in the southwestern mountainous area. The cloud frequency is also prominently high in a small region located northwest of Lake Kasumigaura. These clouds seem to be formed by Mount Tsukuba, an isolated mountain with the height of about 900 m.

The shape of the higher-frequency area in the ellipse of Figure 2.3b shows an excellent fit

to the urban area shown in Figure 2.3a, including the radial urban areas. The low-level clouds negatively correlate well with the NDVI in this area. This is direct evidence that the low-level clouds are more easily formed over urban areas than over rural areas.

The low-level cloud frequency is higher over both the major urban area and the radial urban areas. Especially, the low-level cloud frequency is particularly high over urban areas around Ne (Nerima) and Ur (Urawa), showing a sharp contrast from the rural areas. Station Ne is located in the major urban area but near its northern boundary, while station Ur is located in a narrow rural area between two radial urban areas. The low-level cloud frequency is 26-28% in the radial urban area near Ur, while it is about 25-28% around Ne in the major urban area. The maximum frequency in the entire ellipse is about 30% and is located southeast of Ur, while the lowest one is approximately 18% and is located in the rural area near Ur.

The minimum and maximum values of frequency near Ur, 18% and 28%, correspond to 58 days and 91 days, respectively, in the entire analysis period of 328 days. The difference between the maximum and minimum values is about 3.5 times larger than the square root of the maximum, 91, which can be roughly assumed to be the standard deviation of the ensemble of the estimated maximum frequency from a limited number of samples; therefore, we can conclude that the maximum value is statistically larger than the minimum one.

In spite of a part of major urban area, the low-level cloud frequency is quite low in coastal zones, which are within about 10 km from the coastline. The effects of the coast on the clouds will be discussed later.

Figure 2.4 displays quantitative comparisons between the low-level cloud frequency and the NDVI along Line A in Figure 2.1b. The solid line shows the low-level cloud frequency, and the broken line shows the NDVI. The x-axis indicates the distance from the west edge of Line A. The west side and the east side correspond to the mountainous area and the sea, respectively, and those edges are omitted from Figure 2.4. The station Ur is located at 76 km on Line A. In the figure, the NDVI violently fluctuates along the Line. Arrows a and c indicate the points of the

local maximum NDVI, while arrow b indicates the local minimum NDVI around station Ur. The minimum point corresponds to the center of the radial urban area. The low-level cloud frequency is relatively high at the grids near the minimum point in the NDVI indicated by arrow b, while it is lower at the grids near the maximum NDVI points indicated by arrows a and c. The low-level cloud frequency and NDVI fluctuate in the inverse phase, and their peaks almost coincide; namely, they show a clear negative correlation, while the low-level cloud frequency shifts slightly westward.

Low-level cloud frequency is higher in the mountainous area than in the plain; a phenomenon that is caused by thermally induced local circulations.

2.3. Discussion

The mechanism of the low-level cloud enhancement over the urban area is assumed to be as follows: (1) A stronger sensible heat flux over the urban area enhances the depth of the mixed layer and the height of thermals. In the mixed layer, the potential temperature and specific humidity are almost vertically uniform; as a result, the relative humidity of the top of the mixed layer increases when the depth of the mixed layer increases. Low-level clouds then form at the top of the thermals, since their heights often exceed the lifting condensation level in the mixed layer over urban areas although there is less surface moisture flux. (2) The heat contrast between the urban area and the rural areas generates thermally induced local circulations that form an upward flow over the urban area and converge moisture to it. These two mechanisms are quite sensitive to both insolation and the synoptic scale wind.

The frequency of clouds and the NDVI are well correlated even in small structures. In Figure 2.4, the peaks of cloud frequency at 81.4 km shift slightly from the peaks of the NDVI at 83.6 km downwind of the prevailing wind, which is the easterly in the area shown in Figure 2.5b, but the deviation is less than approximately one grid interval (2.2 km). Since the assumed

mechanism (2) seems to give a larger deviation between the land surface and cloud formation because of the larger horizontal scale of the wind system, the thermals released from the urban area into the mixed layer are more likely to contribute to the cloud formation.

The enhancement of the urban cloud formation is much clearer on calm and clear days, when a typical wind pattern is often observed in the Kanto Plain, as shown by Fujibe (2003). Figure 2.5a shows the low-level cloud frequency on the 74 days that were selected according to the criteria that the Kanto Plain was covered by the typical wind system mentioned above.

In this figure, the shape of the high-frequency area in the plain fits the shape of the urban area much better than in Figure 2.3b, especially over the radially extending urban areas around the station Ur. However, the low-level cloud frequency is still quite low in the coastal area. The contrast in the cloud frequency between the inland urban area and the urban area along the coastline is more conspicuous. The cloud-suppressed area extends more inland in the northwest of Tokyo Bay than that in Figure 2.3b. Figure 2.5b is a composite of the wind system on the calm days mentioned above. An easterly wind covers the northern part of the Kanto Plain, while a southerly wind covers the southern part. A sea breeze prevails in the west of Tokyo Bay. The sea breeze suppresses the height of the mixed layer, since no mixed layer forms over the bay and an internal boundary layer develops over the land surface near the coastline.

Using a numerical simulation, Kusaka et al. (2000) demonstrated that land-use alteration during an 85-year period (1900-1985) modified the wind system over the Kanto Plain. They suggested that the urban effects enhance horizontal convergence around the urban area. This idea is also supported by Fujibe (2003). The wind system in Fig. 2.5b is similar to those previous studies.

The low-level cloud frequency is prominently enhanced along the outer edge of the coastal suppressed area. The enhanced area roughly overlaps with the convergence area of the sea breeze front along the northwestern coast of Tokyo Bay (see Figure 2.5b). The enhancement of the cloud frequency extends over the eastern coastline of the bay as well, where surface winds also

converge. Over the eastern coastline of the bay including Ch, surface winds prominently converge. A sea breeze from the Pacific Ocean across Boso Peninsula rushes against the sea breeze.

2.4. Summary

The horizontal frequency distribution of low-level clouds is estimated around the Tokyo metropolitan area using NOAA satellite images obtained on summer days without regional-scale cloud cover from 1200 to 1500 LST during an 11-year period. The urban area can be determined by the NDVI obtained by the same satellite.

The frequency of low-level clouds is higher over the urban area than the rural areas in the early afternoon; in particular, cloud formation is reinforced over the radially extending urban areas along the major highways or railroads from Tokyo. The distributions of NDVI and the frequency of low-level clouds correlate well within a shift of only about 2 km. This implies that low-level clouds form at the top of the thermals in the mixed layer enhanced by a stronger sensible heat flux in the urban area. A stronger sensible heat flux over the urban area enhances the depth of the mixed layer.

The frequency of the low-level clouds is low in the coastal urban zone located within about 10 km from the coastline. The bay and sea breezes seem to suppress the height of the mixed layer. The urban effects on cloud formation are weaker than those by the land-sea contrast and mountains.

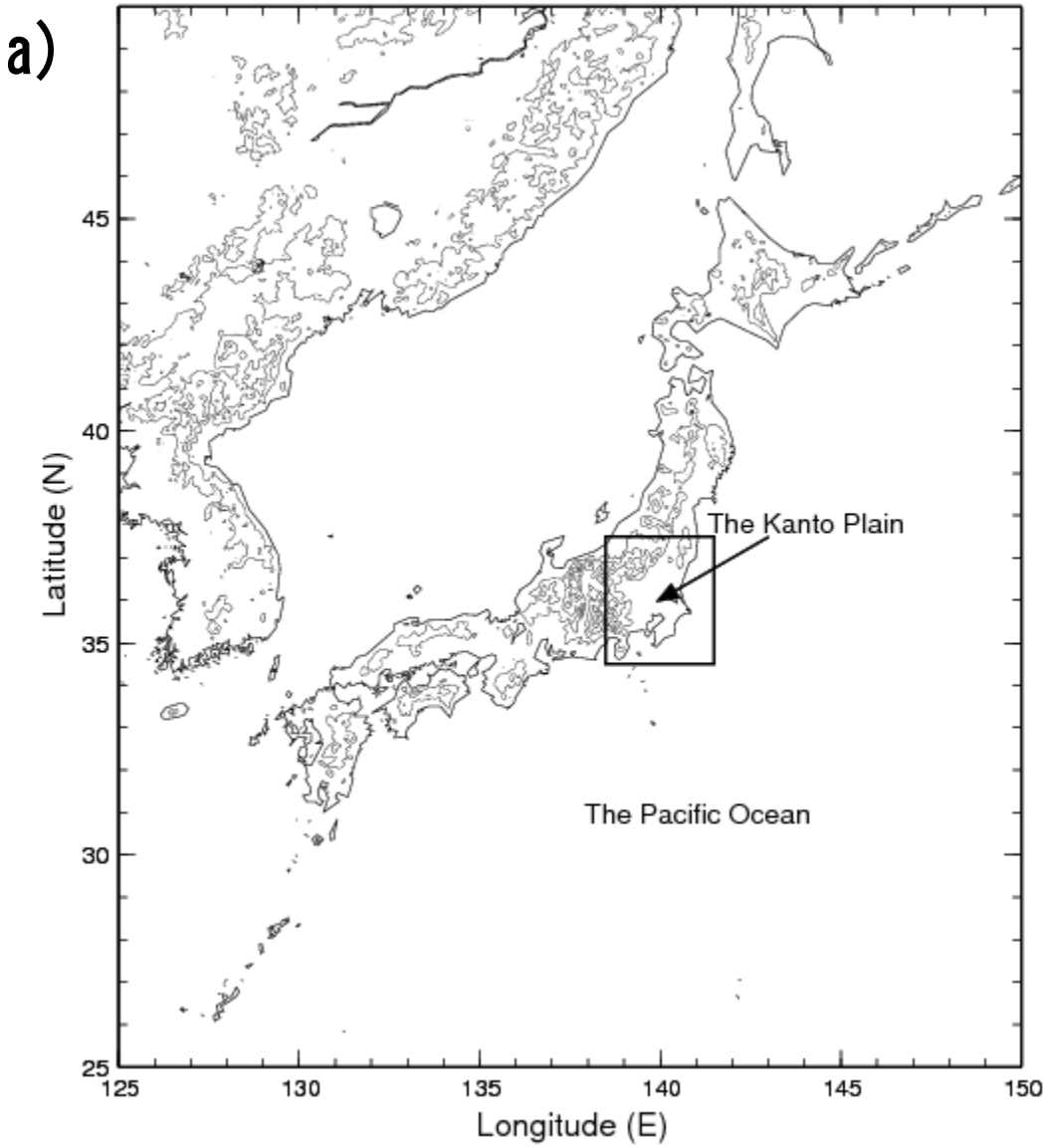

Figure 2.1a: The location of the study area. The rectangle indicates the analysis area of this section, which corresponds to Fig. 2.1b.

b)

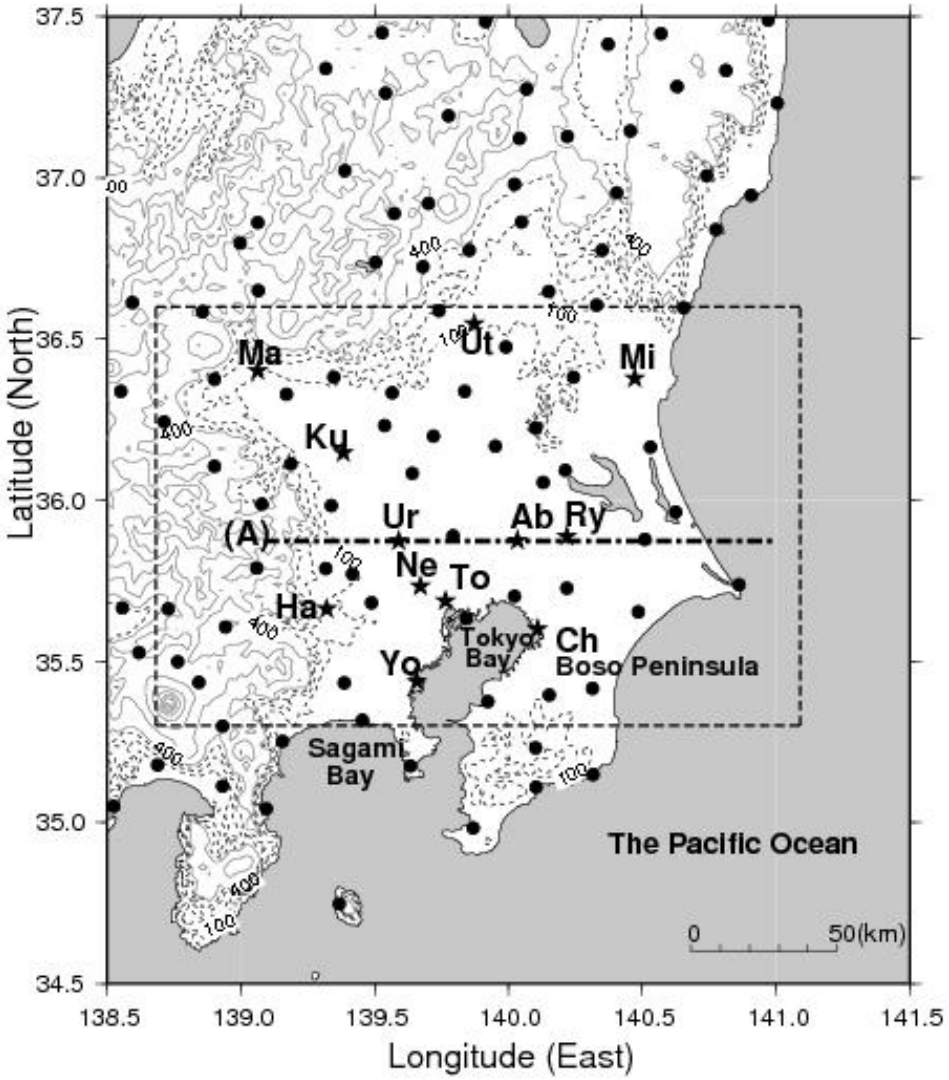

Figure 2.1b: Analysis area and surface observation stations. Circles and stars indicate AMeDAS surface observation stations. Only stars are used in Figures 2.3 and 2.5. The box with broken lines indicates the analysis area of cloud frequency. The shaded areas indicate water surface. The contour of the broken lines shows ground surface elevation of 100 m, and the interval of solid lines is 400 m.

c)

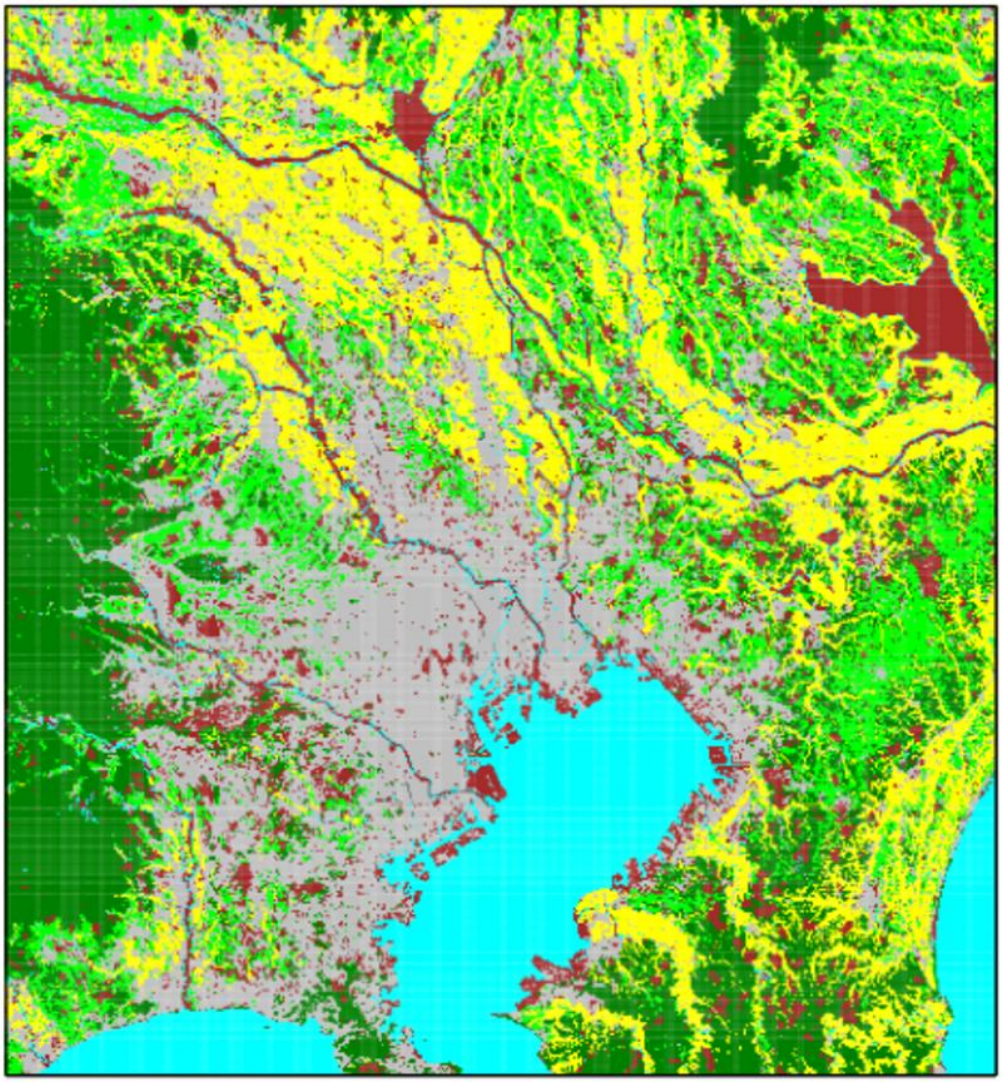

Figure 2.1c: The land use in the Kanto Plain. Gray, yellow, light green, dark green, light blue, and brown indicate urban and residential area, paddy field, other field, forest, sea and river, and other land use, respectively. The land use data is supplied by Ministry of Land, Infrastructure and Transport, Japan.

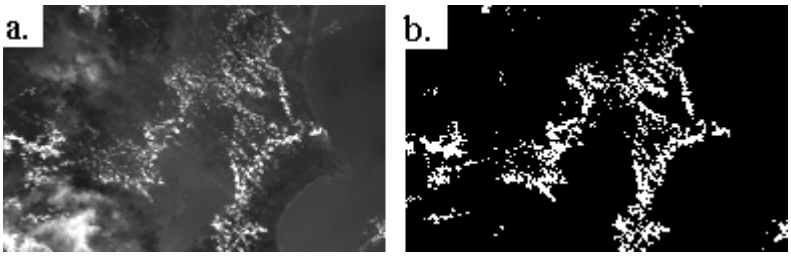

Figure 2.2: Comparison between (a) NOAA Channel-1 data image and (b) two-value data image on the sample day (2 August 1990). The former is shown in a gray scale of 256 levels (a whiter pixel means higher reflectance).

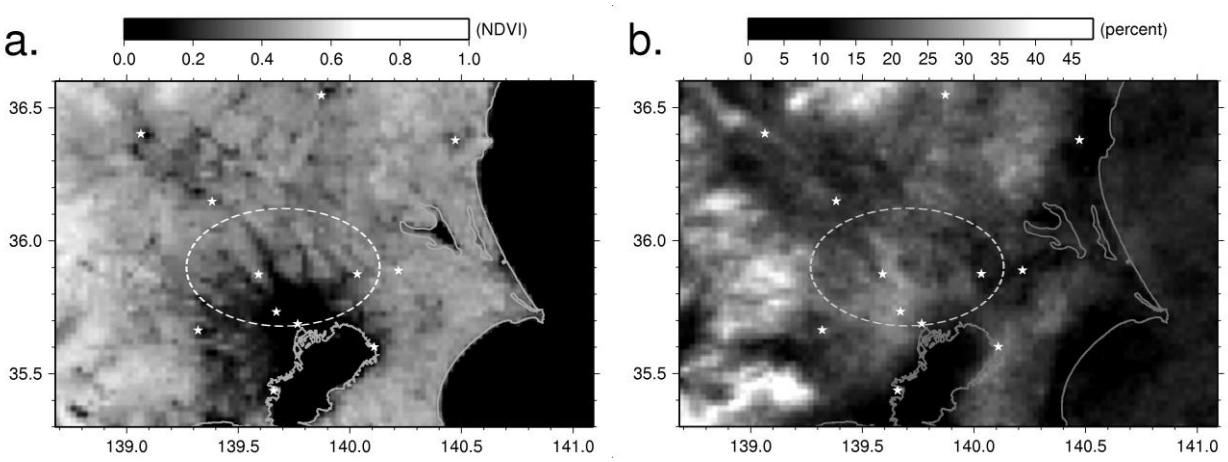

Figure 2.3: (a) NDVI during summer in 1991; (b) Low-level cloud frequency on 328 clear summer days. Lighter shading means higher NDVI and higher low-level cloud frequency. The ellipses shown in broken lines indicate the characteristic urban areas that are the main focus of this study. The stars are the same as those in Figure 2.1b.

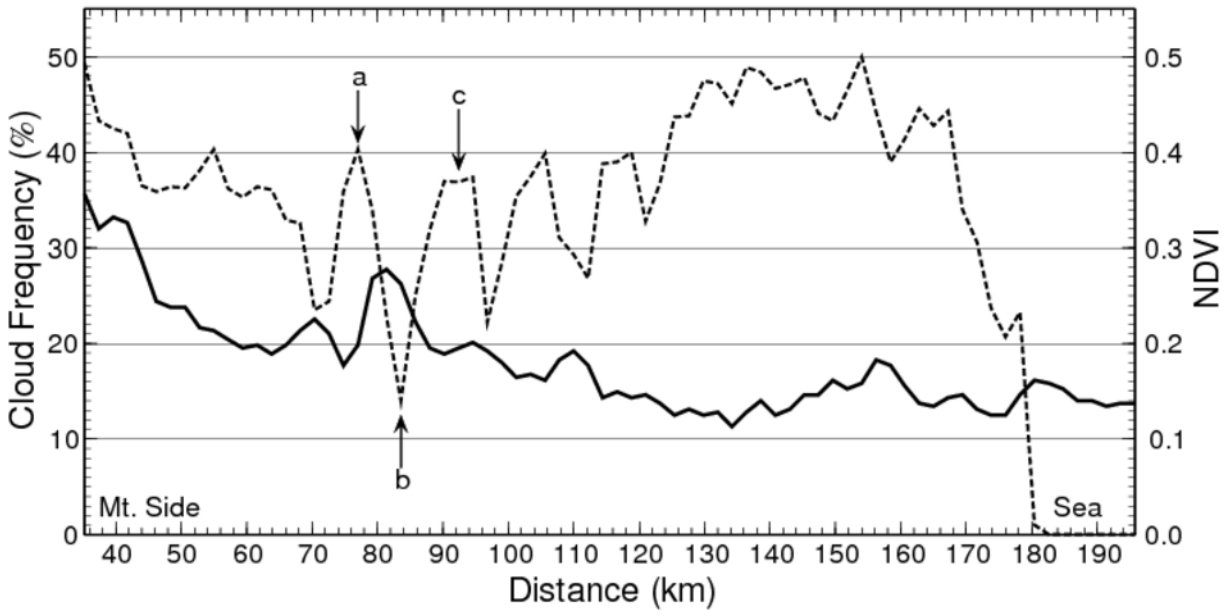

Figure 2.4: Low-level cloud frequency versus the NDVI along Line A in Figure 2.1b. The solid line shows the low-level cloud frequency, and the broken line shows the NDVI. Lower NDVI indicates an urban area. The x-axis indicates the distance of the west edge of Line A. Arrows a-c indicate the peaks of the NDVI near Ur at 76 km.

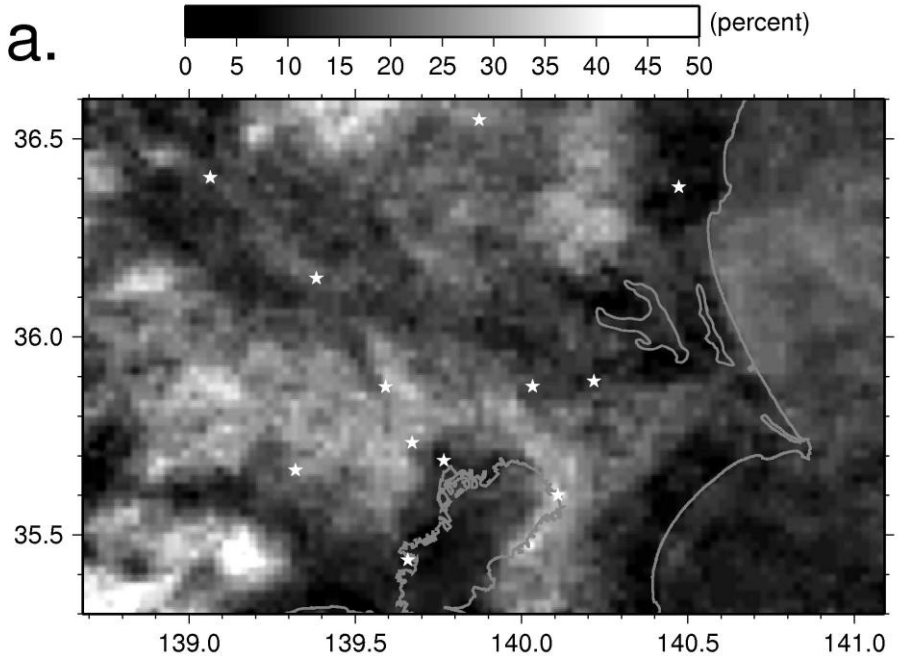

Figure 2.5: (a) Low-level cloud frequency in a case of typical wind systems.

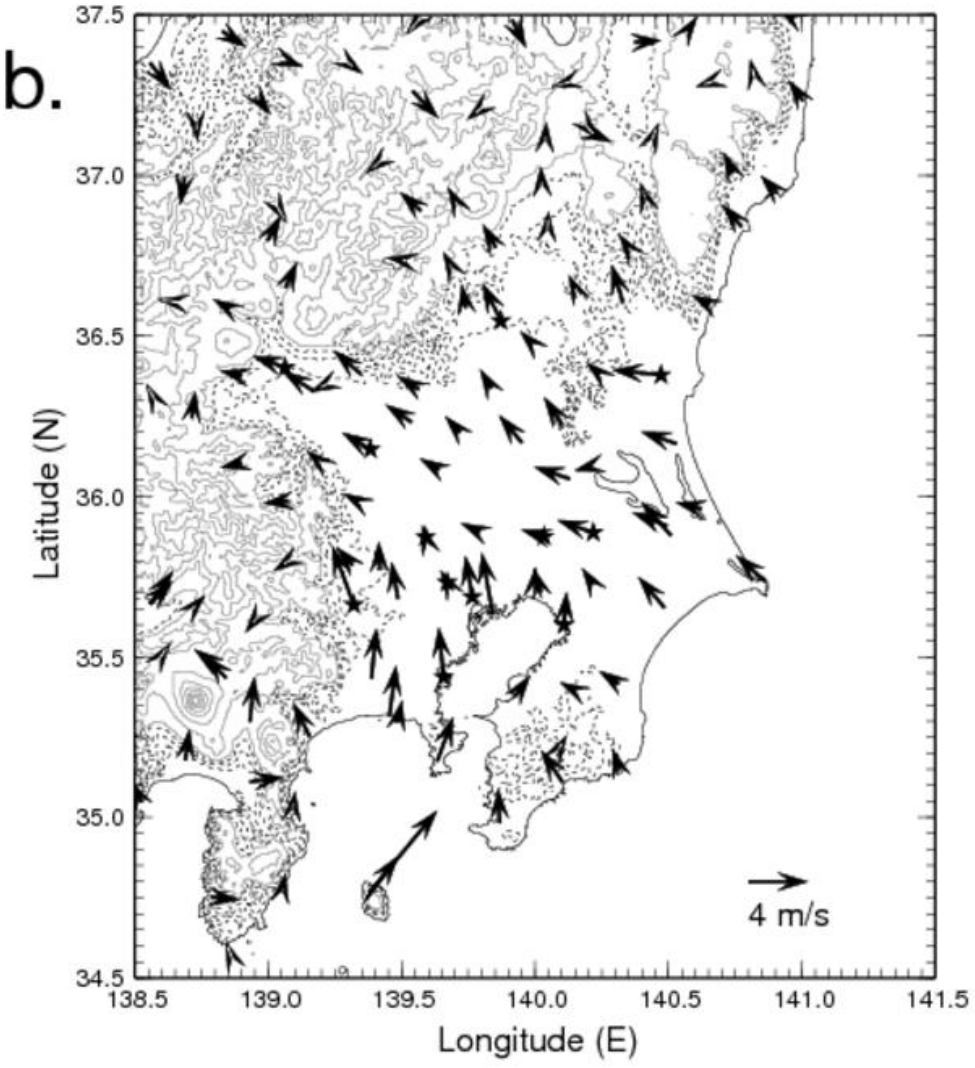

Figure 2.5: Continued. (b) Composite of surface winds on 74 days categorized into the wind system, of which the local winds are prominent.

3. Observation of time variation of convective clouds over urban area

The difference of cloud frequency between the urban and rural areas over the Kanto Plain in summer is revealed in Section 2. The difference is significant around Saitama City in northern Tokyo, where the urban and rural areas exist alternately, in the analysis, but the features of the urban clouds and the mechanisms of the cloud difference are unknown. To investigate the features of the urban clouds, the ground-based photographic observation of the urban clouds was conducted around the area.

3.1. Method of ground-based photographic observation

The urban clouds investigated in Section 2 can be classified into cumulus clouds, because the horizontal scales of most of the urban clouds are within a few kilometers in each NOAA satellite image. The satellite data is insufficient in the time resolution for investigating the time variation of small cumulus clouds whose lifetime is always much shorter than one hour. Thus, a digital camera was selected as an instrument for observing the urban clouds from the ground level.

The camera was set toward east-northeast to shoot the urban clouds at two-minute interval. The observation point is Fujimi Fire Department, which is located at 139.550°E, 35.858°N in Fujimi City, Saitama Prefecture and is indicated by the double circle in Figure 3.1. Gray shade indicates urban areas and the solid line indicates railroads in Fig. 3.1. The observation period is from late July to early September in 2003, 2004, and 2005.

The supplemental surface meteorological observation was also conducted on some of

those days. Surface air temperatures and radiation temperatures (surfaces, skis, and cloud bases) were measured by Assmann aspiration psychrometers and handy spot thermometers (MINOLTA HT-10D), respectively. In addition, the sky view camera was operated on a few days.

Images of the Moderate Resolution Imaging Spectroradiometer (MODIS) aboard the Terra and Aqua satellites were used for observing the horizontal distribution of clouds in the Kanto Plain. Each satellite observes the same area once a day in the daytime. Their horizontal resolution of visible images is 250 m, which can resolve a single cumulus cloud.

3.2. Observed urban clouds

3.2.1. Time variation of urban clouds on a typical day

Figures 3.2 indicate the time variation of clouds over the urban area on a typical day, 4 August 2003. The urban clouds were clearly observed by the camera on the day, furthermore the two satellite images of MODIS also observed the clouds. Cumulostratus covered the entire area from about 0600 LST to around 0830 LST, and then the area was almost clear from 0830 LST to 0930 LST (Fig. 3.2a). After 0930 LST, small cumulus clouds formed over the urban area. On the other hand, no cloud existed around the observation point (Fig. 3.2b).

Figure 3.2c shows a photograph of the urban cloud, which was shot during scanning of MODIS images shown in Fig. 3.3a, and small clouds still formed over the urban area. In figure 3.3, dark gray, green and dark blue indicate the urban areas, the vegetated areas and the water surface, respectively. The yellow circle indicates the observation point. The vegetated areas roughly correspond to the higher value of NDVI in Fig. 2.3a. The wedge-shaped vegetated area exists on the east of the observation point. On the other hand, the long urban area extends along JR Takasaki Line, which is indicated in Fig. 3.1, on the east of the vegetation area. The urban area mainly consists of Saitama City.

In the Fig. 3.3a, many small cumulus clouds form a cloud line on the long urban area,

whereas no cloud forms in the vegetated area. Since the satellite image shows no cloud between the observation point and the urban area along the JR Takasaki Line, the cloud line shown in Fig. 3.2c can be identified as the urban cloud above the long urban area in the satellite image. The height of the cloud base is roughly estimated to be 1 km, while the depths of the clouds are quite shallow in Fig. 3.2c. In addition, the wind was almost calm in the center of the plain at the time, while Boso Peninsula was covered by strong southwesterly and there are many cloud lines induced by roll-convections.

The urban clouds began to develop clearly at 1046 LST (Fig. 3.2d). Figure 3.2e shows the same clouds at 1116 LST. The shape of the clouds implies that the top of the cloud exceeds the level of free convection (LFC). The cloud base is almost same as Fig. 3.2a, but the cloud top seems to be nearly 2 km. The clouds at 1132 LST shown in Fig. 3.2f have developed much more higher than those of 1116 LST, and then became Cumulus congestus. The height of the cloud top became the maximum at about 1210 LST during scanning of the satellite image of Aqua/MODIS shown in Fig. 3.3b. The development of the urban clouds is also seen in Fig. 3.3b. After that, the urban clouds have gradually decayed, and then those clouds have completely disappeared at around 1400 LST.

MODIS images of the urban clouds on some of other typical days are shown in Fig. 3.4a at 1220 LST on 13 August 2004, Fig. 3.4b at 1250 LST on 1 September 2004, Fig. 3.4c at 1230 LST on 14 August 2005, and Fig. 3.4d at 1325 LST on 29 August 2005. The day of Fig. 3.4b will be described in Section 3.2.3. The original image data is obtained from the web site: http://rapidfire.sci.gsfc.nasa.gov/subsets/

3.2.2. Features of time variation of urban clouds

The urban clouds were observed on 12 days in 54 days when photographs were taken. The photographic observation on the 12 days are summarized as follows; In most cases, the onset time of the urban clouds is between 0800 LST and 1130 LST and the dissipation time is between

1300 LST and 1700 LST, although the time variation of clouds somewhat depended on days. The duration of the cloud forming ranges between 3 to 6 hours in the most days. Those clouds are generally "active cumulus clouds" defined by Stull (1985). The clouds gradually developed, and then the tops of the clouds penetrate into LFC in most of the days; they become Cumulus congestus in the early afternoon on some of those days, although they have never grown to Cumulonimbus in the photographic observation.

3.2.3. Meteorological observation

The meteorological observation was conducted on 4 days in 2004, which are 21 July, 6 August, 22 August, and 1 September. The urban clouds formed on two of the days, 6 August and 1 September, although the appearance of urban clouds was unclear on 6 August.

The urban observation points in office areas of Saitama City, Saitama Prefecture, were Sakuragi Elementary School (139.617°E, 35.903°N) on 6 August and in front of the Saitama Central Ward Office (139.627°E, 35.884°N) on 1 September. On the other hand, AMeDAS Saitama station (139.585°E, 35.875°N) was assumed to represent a rural point.

Many cloud lines induced by roll-convections covered the entire observation area in the morning on 6 Aug. 2004. Those cloud lines disappeared around noon. After that many small clouds still generated over the urban area, in contrast a few small clouds generated the rural area. The lifetime of the rural clouds ranges from 4 to 6 minutes, on the other hand, that of many of the urban clouds is more than 10 minutes. The urban clouds were classified into "forced cumulus clouds" (Stull, 1985) on the day. The meteorological observation period was from 0800 LST to 1600 LST. The observed results are shown in Fig. 3.5. The air temperatures of the urban and the rural points have been almost the same when the area was covered by the many cloud lines. After only the urban clouds generated, they were 36.0 ℃ and 33.5 ℃ at 1300 LST, respectively, and the difference of temperatures was maximum at that point.

On 1 September, the observation was conducted from 0930 LST to 1700 LST. The entire area was very cloudy early in the morning, and then it was completely clear in the middle of the morning. The first urban cumulus cloud appeared clearly at 1120 LST, which is shown in Fig. 3.6. After that, the number of the urban clouds gradually increased, and then the urban cloud line was formed at 1252 LST (shown in Fig. 3.7). The cloud line is also confirmed by the satellite image of Fig. 3.4b (139.5-139.7°E, 35.8-36.0°N). The clouds were classified into "forced cumulus clouds" until 1430 LST. Some cumulus clouds appeared intermittently over the rural area from 1330 LST to around 1445 LST. The urban clouds changed into "active cumulus clouds" after 1430 LST. The activities of the urban clouds gradually weakened after 1600 LST. The dissipation time of the urban clouds was 1712 LST. Figure 3.8 shows the time series of the air temperatures of the urban and the rural points. The difference between the air temperatures of urban and rural was 2.9 K and 2.4 K at 1000 LST and 1400 LST, respectively. The urban heat island existed through the observation period on the day. Figure 3.9 shows the radiation temperature of the road (asphalt) and the grass surfaces in the office area, which locate in front of the Saitama Central Ward Office. The road surface temperature exceeded 55 ℃ at 1300 LST, while the grass surface has kept under 42 ℃.

The air temperature in the urban area was higher than that in rural when the urban clouds were forming, although the meteorological observation data is limited. The radiation temperature of the road was much higher than that of the grass in the observation. Generally, urban areas are mainly constructed from artificial materials like roads whose evaporation is much less than vegetations. The influence of anthropogenic heat is relatively small in summer because of the strong downward short wave radiation (Ichinose et al., 1999). It is speculated that the sensible heat flux is large in the urban area; as a result the higher air temperature in the urban lower atmosphere become the trigger of thermals, and thus the small clouds tend to form over the urban area.

3.3. Summary

To investigate the features of the urban clouds, the ground-based photographic observation of the urban clouds was conducted around Saitama City, where the difference of cloud frequency between urban and nearby rural areas is the sharpest. The urban clouds were observed on 12 days in 54 days when photographs were taken. The horizontal cloud distribution was observed by MODIS images and the urban clouds in the pictures were confirmed to form over the urban area.

In most cases, the onset time of the urban clouds was between 0800 LST and 1130 LST and the dissipation time was between 1300 LST and 1700 LST, although the time variation of clouds somewhat depended on days. The duration of the cloud forming ranged between 3 to 6 hours in the most days. Those clouds were generally "active cumulus clouds". The clouds gradually developed, and then the tops of the clouds penetrated into LFC; they became Cumulus congestus in the early afternoon on some of those days.

On one of typical days, 1 September 2004, some meteorological observation was conducted. The urban heat island, which was about 2 K, has continued to exist from before the onset of the first urban cumulus cloud to the cloud dissipation time.

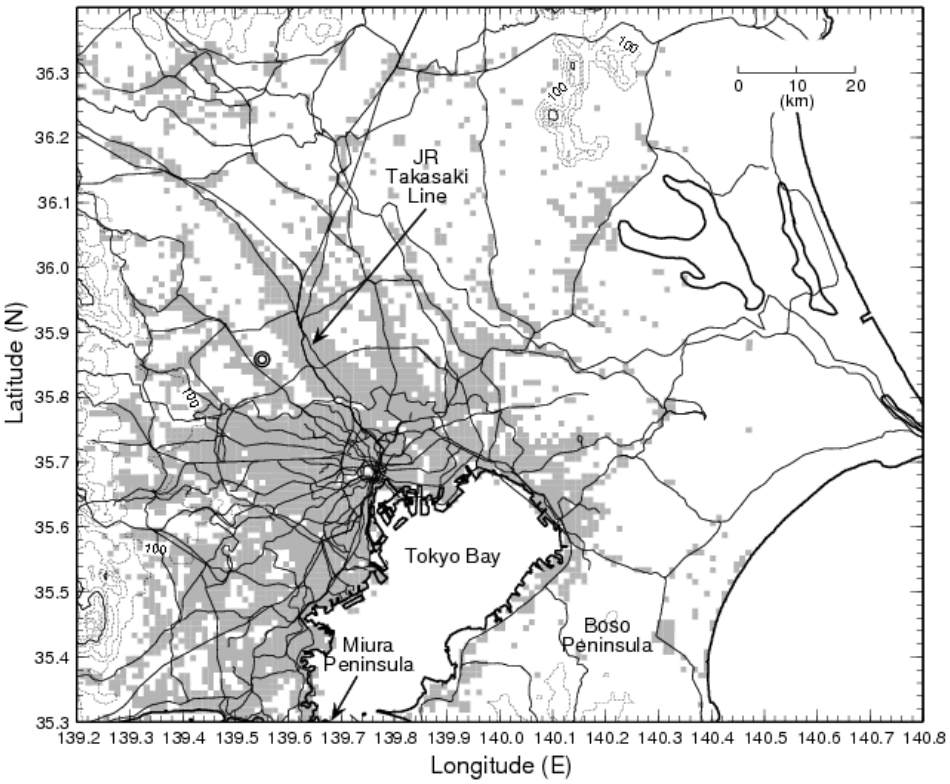

Figure 3.1: The domain of analysis. The double circle indicates the ground-based photographic observation point. Gray shade indicates the urban areas. Solid lines indicate railroad lines. Dotted lines and thin solid line indicate the contours of 100 m interval and of 500 m interval, respectively.

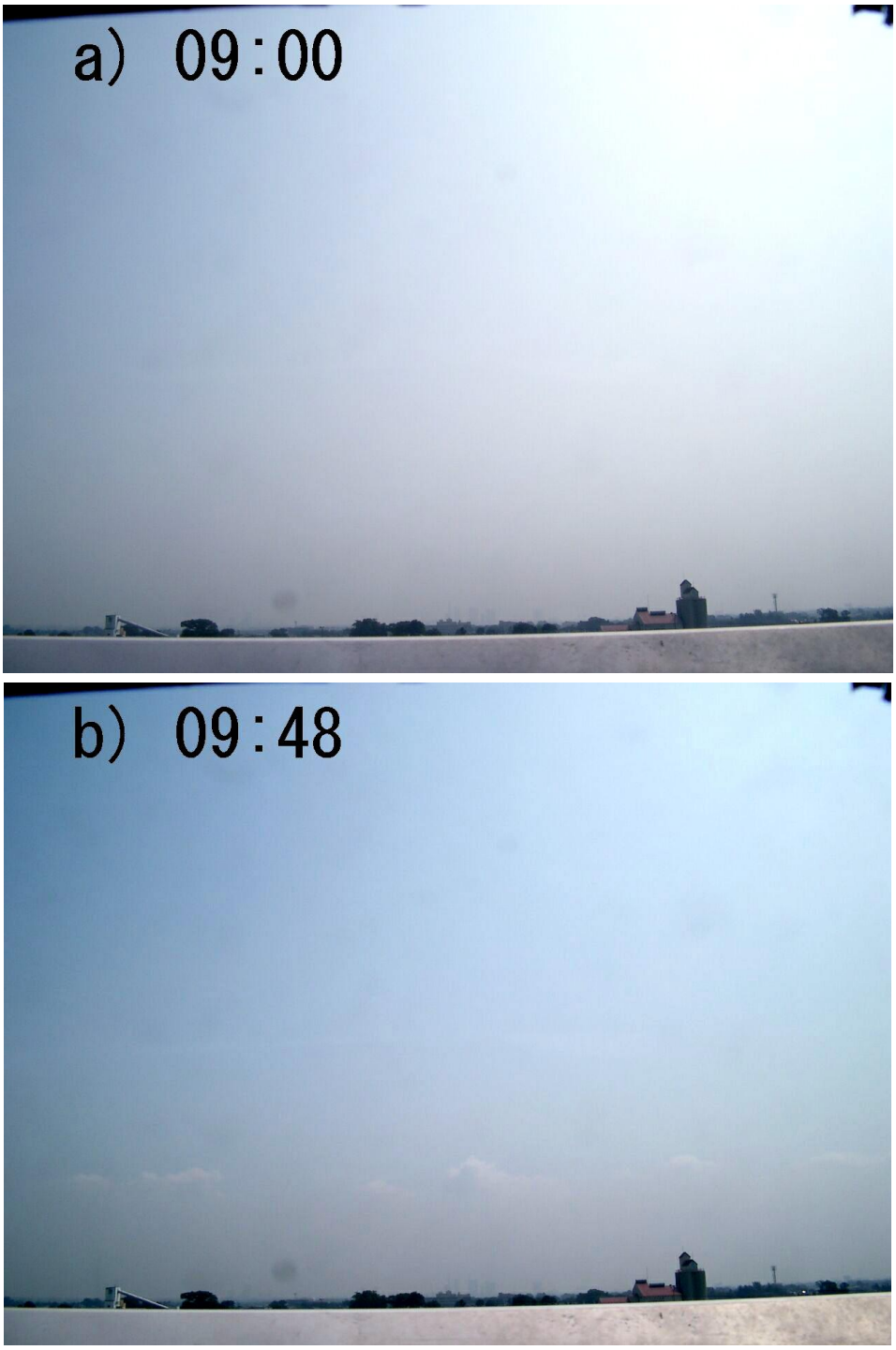

Figure 3.2: The pictures of the urban clouds over Saitama city on a typical day of 4 August 2003, observed at (a) 0900 LST and (b) 0948 LST.

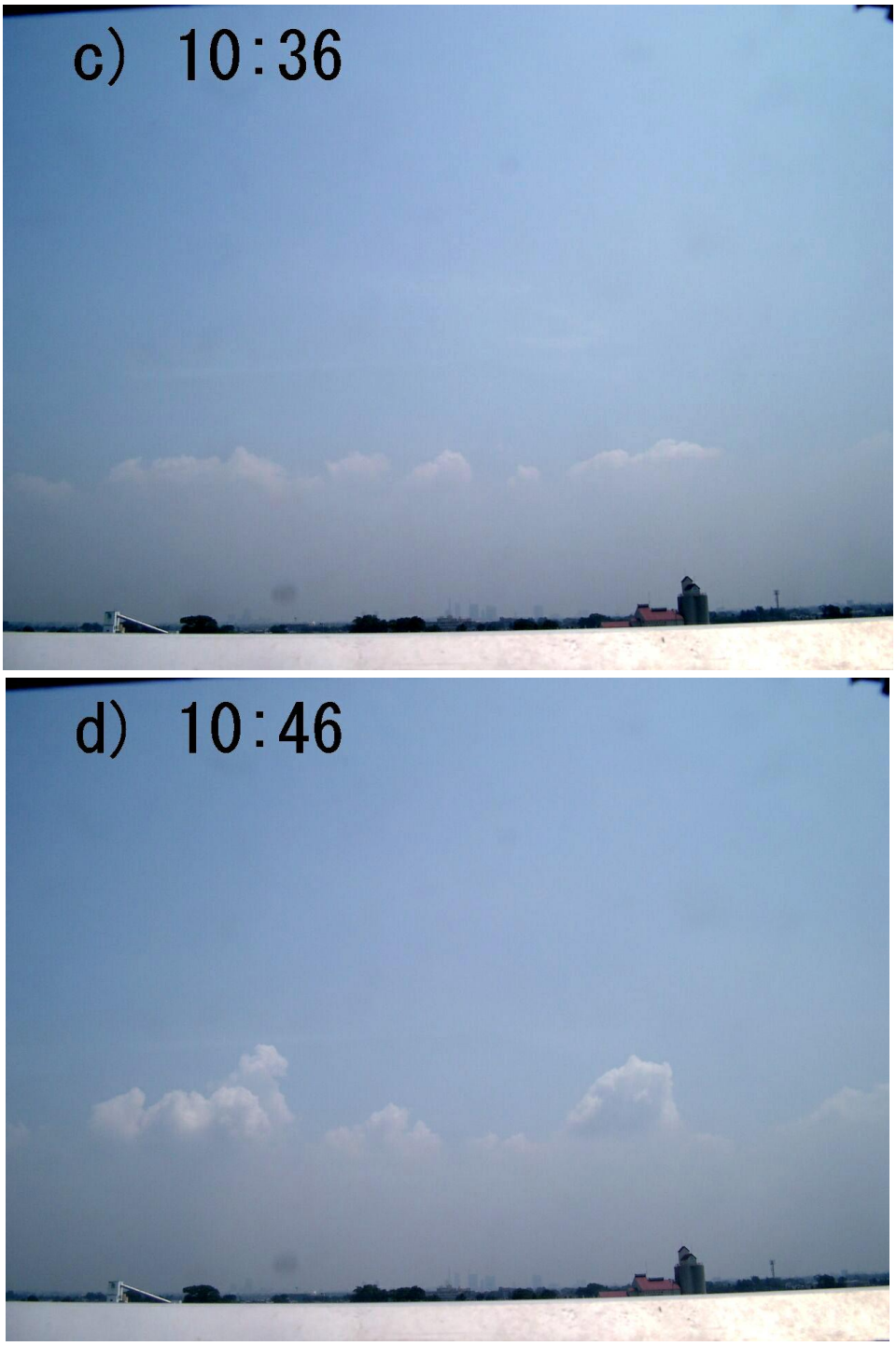

Figure 3.2: Continued. (c) 1036 LST and (d) 1046 LST.

Figure 3.2: Continued. (e) 1116 LST and (f) 1132 LST.

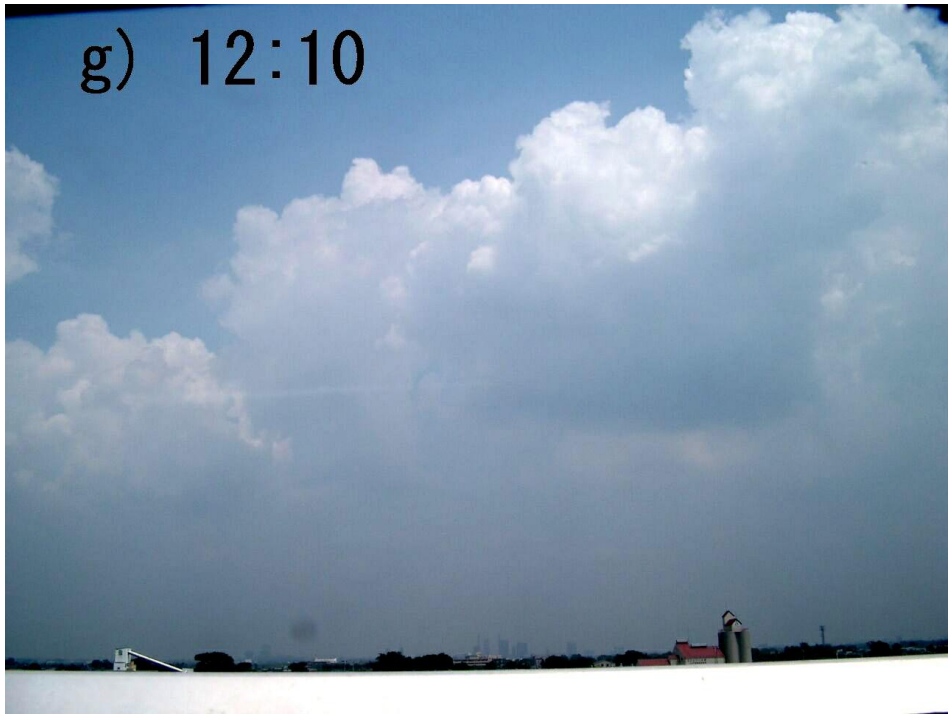

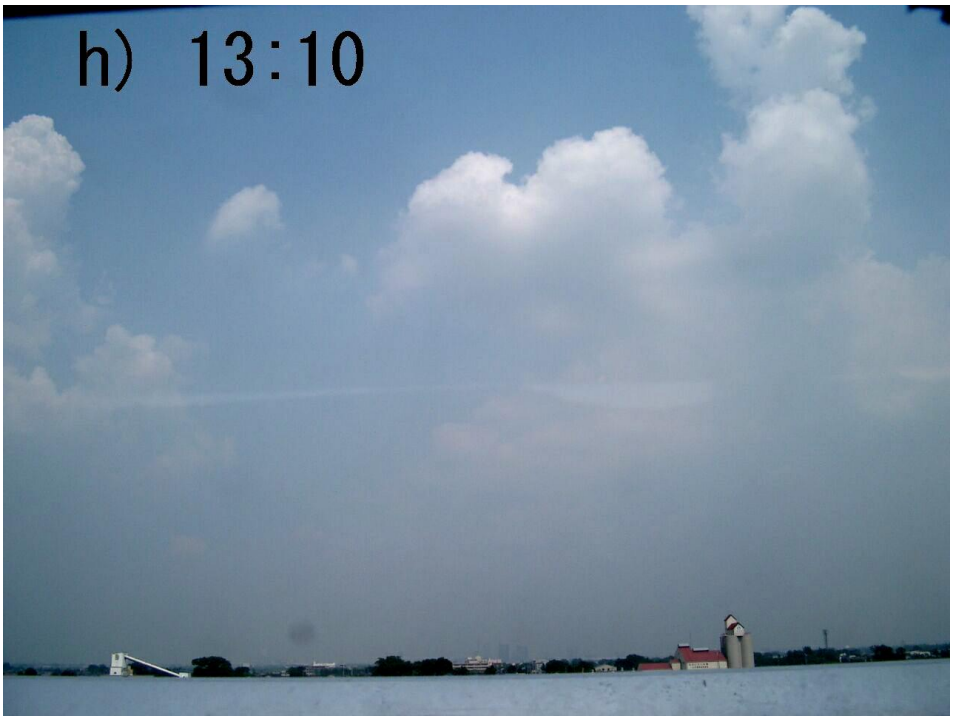

Figure 3.2: Continued. (g) 1210 LST and (h) 1310 LST.

Figure 3.2: Continued. (i) 1354 LST.

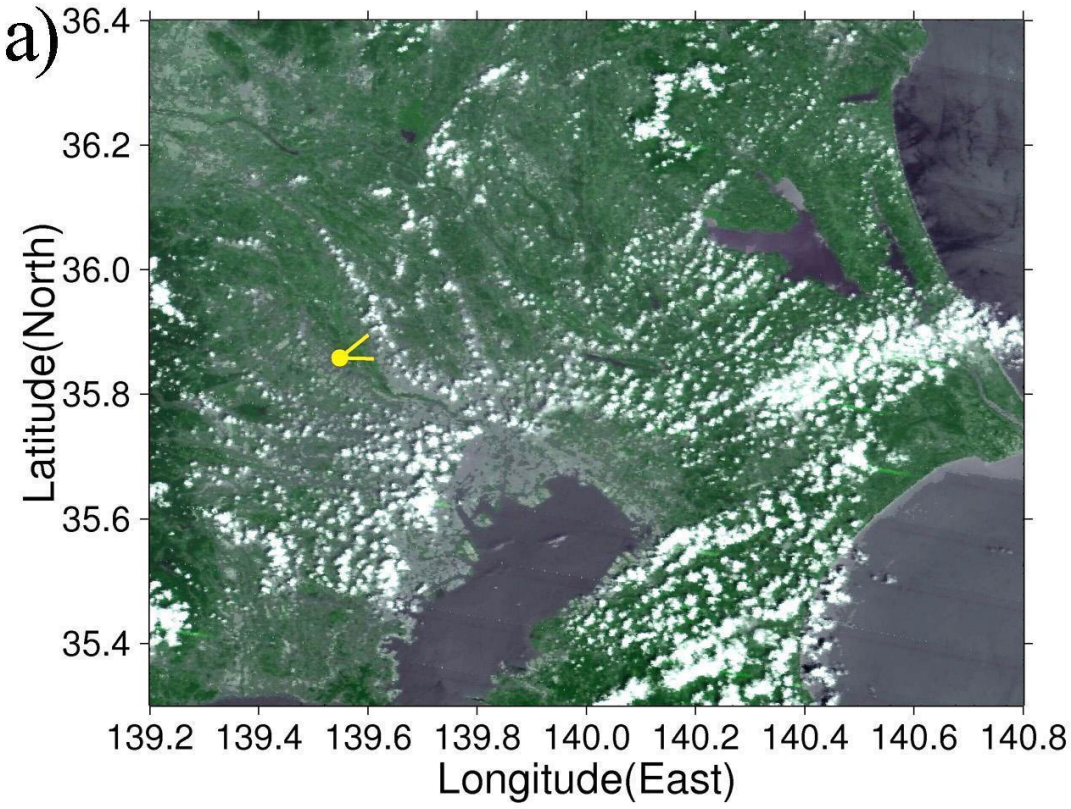

Figure 3.3: The satellite images on a typical day of 4 August 2003. (a) Observed at 1035 LST by Terra/MODIS. The yellow circle indicates the photographic observation point.

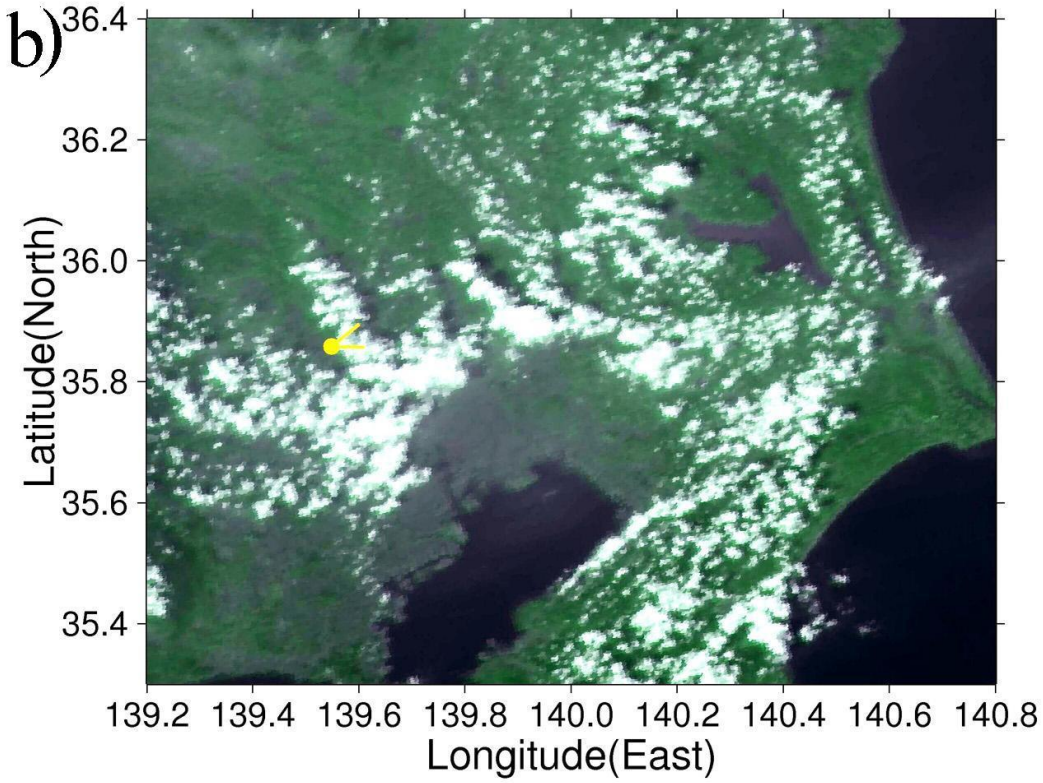

Figure 3.3: Continued. (b) Observed at 1210 LST by Aqua/MODIS.

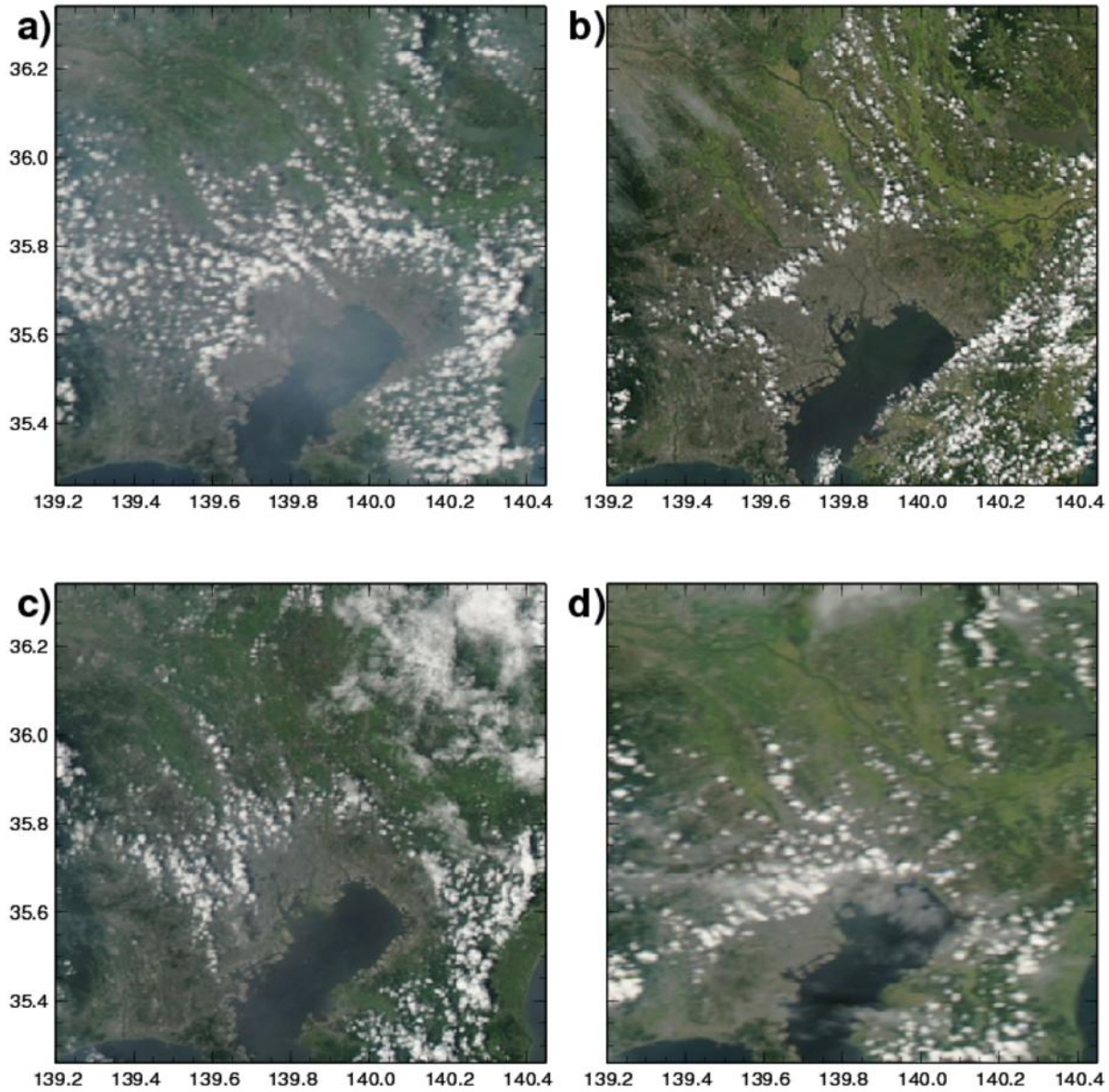

Figure. 3.4. Aqua/MODIS images of urban clouds on other typical days, (a) at 1220 LST on 13 August 2004, (b) at 1250 LST on 1 September 2004, (c) at 1230 LST on 14 August 2005, and (d) at 1325 LST on 29 August 2005. The original image data is obtained from the web site: http://rapidfire.sci.gsfc.nasa.gov/subsets/

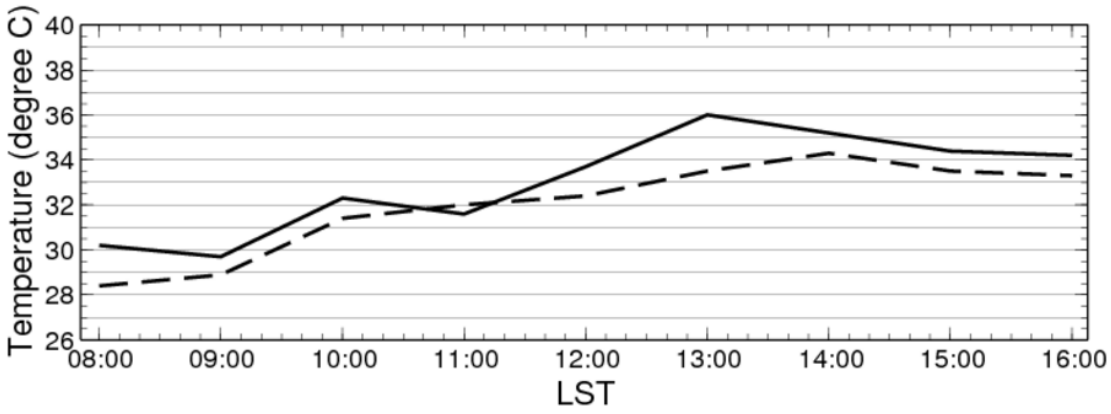

Figure 3.5: The time series of the air temperatures on 6 August 2004. The solid and dashed lines indicate the temperatures of the urban observation point (Sakuragi Elementary School) and the rural point (AMeDAS Saitama), respectively.

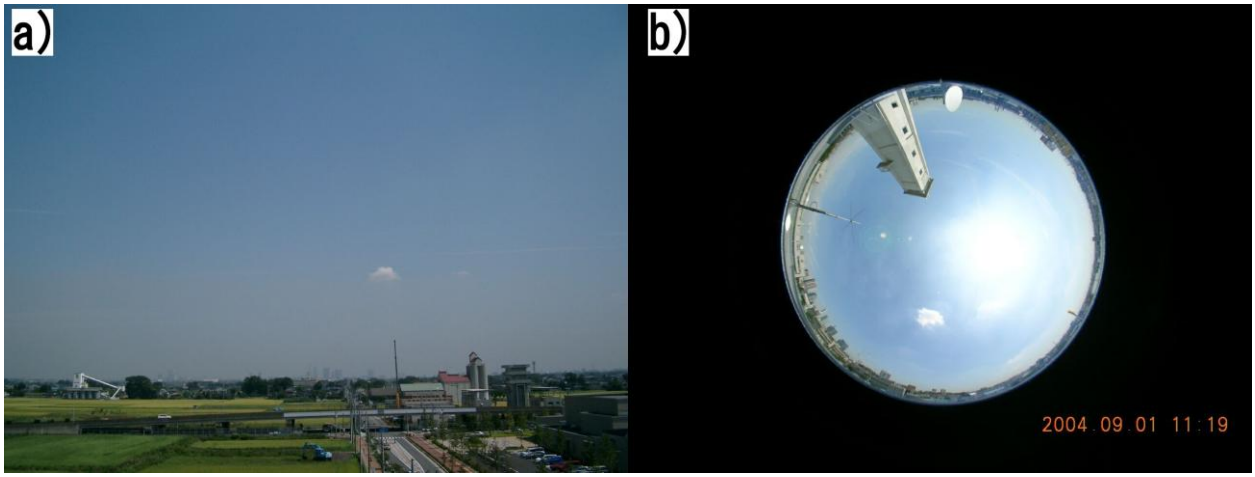

Figure 3.6: The photographs of first cumulus cloud at 1120 LST on 1 September 2004 taken by (a) the camera horizontally at Fujimi Fire Station and (b) the sky view camera in the middle of the city. Upper side is the north and right side is the east in (b).

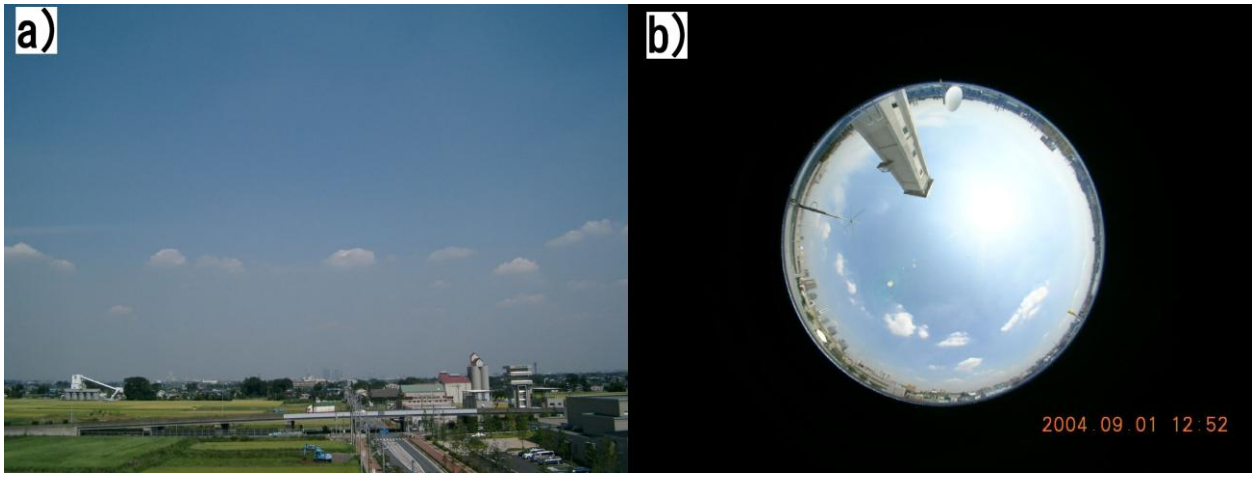

Figure 3.7: Same as Fig. 3.6 except for the photographs of cumulus cloud line at 1252 LST.

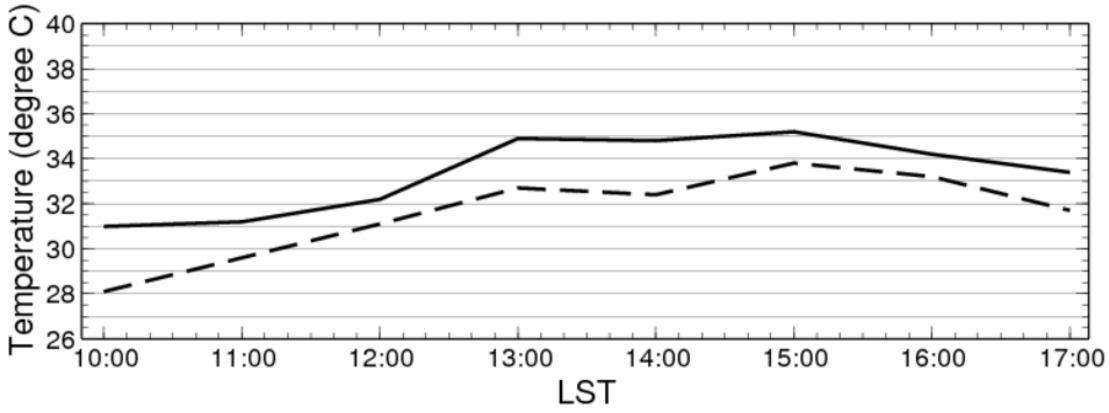

Figure 3.8: Same as Fig. 3.5, but for on 1 September 2004, and the urban observation point is at in front of the Saitama Central Ward Office.

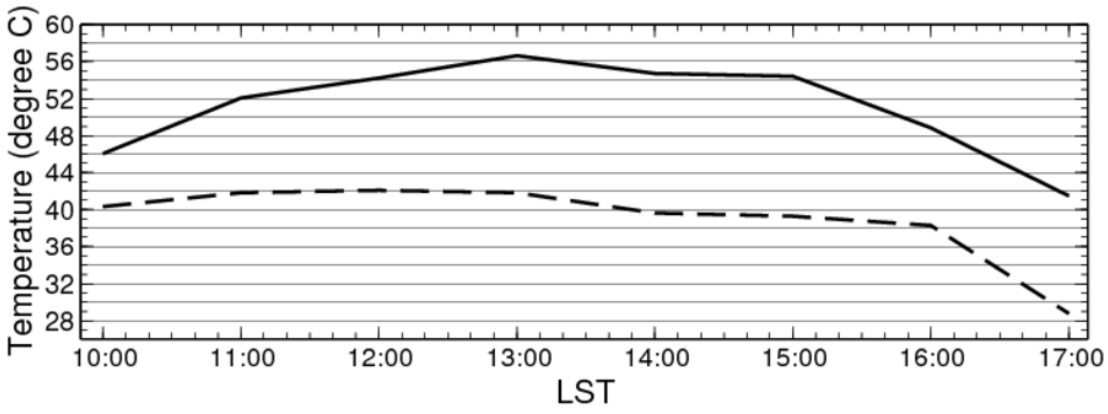

Figure 3.9: The time series of the radiation temperatures on 1 September 2004. The solid and dashed lines indicate the road and the grass of the urban observation point (at in front of the Saitama Central Ward Office), respectively.

4. Numerical experiments on cumulus cloud formation in northern Tokyo

In the previous section, the features of the urban clouds are comprehended by the observations, but the mechanism of the cloud contrast between the urban and the rural areas is still unclear. In this section, the urban clouds will be simulated by a three-dimentional numerical model, and the mechanisms will be investigated to conduct some sensitivity experiments.

4.1. Methods

4.1.1 Numerical model and experimental design

The numerical model used in this study is a modified version of Regional Atmospheric Modeling System (RAMS). This model (TERC-RAMS) is originally developed at Colorado State University (Pielke et al., 1992) and modified at the Terrestrial Environment Research Center, University of Tsukuba. The horizontal grid interval is 1 km in the fine grid system (122×122 grids), which is nested in the coarse grid system that covers central Japan with 5 km resolution. The fine grid is centered at 35.8°N, 139.8°E. The domain is showed in Fig. 4.1. The vertical gird interval is 30 m in the lowest layer. It stretches up to 800 m in the upper layer and the height of the top of atmosphere is set 16 km. Turbulent parameterization is given by Mellor and Yamada 2.5-level, which is a TKE turbulent model. Microphysics is parameterized by Tripoli and Cotton (1980) and Chen and Cotton (1988) in which water substance are decomposed into seven components. The radiation scheme in the original RAMS version 3b was replaced by a precise band scheme presented by Nakajima et al. (2000) in the model. The Klemp and Wilhelmson (1978) scheme is used as lateral boundary condition in this study. Condensation and radiation effects of the urban aerosol were assumed to be negligible.

It is better to apply large eddy simulations for thermals and small fair-weather clouds around the top of the mixed layer. Zhu and Albrecht (2003) studied the basic physics underlying fair-weather clouds by large eddy simulations assuming a horizontal grid interval of 100 m. The large eddy simulation can explicitly represent thermals and small clouds as microscale processes. But it is difficult to cover wide area enough to simulate local circulations induced by the topography in realistic simulations. Actually, distribution of fair-weather clouds is strongly affected by thermally induced local circulations, i.e., land and sea breezes, and mountain and valley winds. Avissar and Liu (1996) stated that upward motion of the mesoscale circulations generated by landscape heterogeneities is stronger than that induced by microscale circulations such as thermal cells, suggesting that fair-weather clouds can be roughly simulate by mesoscale numerical models whose grid interval is 500 m. TERC-RAMS is a mesoscale model with 1-km grid interval which cannot simulate microscale disturbances, but it covers wide area and is able to simulate most of the mesoscale circulations including orographically-induced local circulations.

Land use is classified into two categories, urban and rural, by using the land-cover data with 100-m resolution supplied by Ministry of Land, Infrastructure and Transport, Japan. The data surveyed in 1997 was classified into 11 land-use classification, e.g., the paddy fields, other agricultural lands, the forests, the building sites, the water surface. Only the building sites are assumed to be urban areas and other classes over land are assumed to be rural areas. For the rural areas, vegetation type is assumed to be uniform short grass, while soil type is assumed to be silt-loam. Initial soil water content is assumed to be 0.5 at the layers up to 50 cm, which is defined by the ratio of soil water content and the saturated soil water content. In the urban area, initial soil water content is assumed to be 65 % of that of rural in the control run. We abbreviate the control run as "CTRL" here. The urban effect is expressed only by drier soil surface. Although we have obtained similar cloud distribution even assuming more sophisticated urban canopy model given by Kusaka et al. (2001), the simple urban expression allows us to easily

control sensible heat flux in the urban area. As long as the simulation is limited during daytime, the thermal effects of urban area can be simulated enough accurately for the cloud formation above the urban area.

The fine grid system covers the Kanto Plain, which includes the Tokyo metropolitan area. The plain is surrounded by mountains to the north and the west, while it faces the ocean to the south and the east. Urban areas are indicated by shade in Fig. 4.1. We focus on Region A enclosed by a rectangle with thick solid line in the figure. The region was also focused in Sections 2 and 3. Three long shape urban areas exist in the region. We name these urban areas "extending urban area a, b, and c" and will abbreviate them as "EUA-a, -b, and -c" here. EUA-a, EUA-b, and EUA-c locate in the western part, center, and the eastern part of Region A, respectively. They are indicated by symbols "a", "b", and "c" as shown in Fig. 4.1. EUAs are a kind of satellite cities along railroad extending from the central part of Tokyo. Those urban areas are surrounded by rural areas.

The large and dense urban area, which is enclosed by thin solid lines and a thin broken line, is abbreviated as "LUA" here. While thin solid lines indicate border between prefectures, LUA almost corresponds to the main area of Tokyo metropolitan area.

Figures 4.2a and 4.2b display the vertical profiles of potential temperature and relative humidity, respectively, observed at 'Tateno' station, which is one of the sounding stations of Japan Meteorological Agency locating at the black square indicated in Figure 4.1. The thin lines show the profiles observed at 0900 LST (00 UTC) in the 22 days when the urban clouds were observed by MODIS images. In the Figure 4.2a, potential temperature is shown as the difference from that at 925 hPa in order to show only the static stabilities in those days. Profiles of potential temperature indicate slightly more stable condition than the standard lapse rate, implying that the area was covered by anticyclones.

The thick lines in the figures show the profiles of potential temperature and relative humidity assumed in the model as the initial condition. Initial relative humidity is in the range of

the observed variability but somewhat lower than the mean observed profile, while the dry static stability is slightly stronger stable than that of the mean observed profile. These profiles are assumed in order to avoid unexpected developments of deep convection and precipitation, which would drastically destroy the fair weather condition in a model. The initial horizontal winds are assumed to be uniform southerly wind with the speed of 1 m/s, which is roughly consistent with the synoptic condition in clear calm summer days. The simulation was started at 06 LST (21 UTC) and integrated twelve hours.

4.1.2. Data for comparison with the model results

The simulated cloud distribution will be validated by the comparison with satellite images observed by MODIS aboard the Terra and Aqua satellites. These are provided by Goddard Earth Sciences Data and Information Services Center, NASA. The images are composed by Channel 1 to 4 of MODIS L1B. Resolutions of red and near-infrared channel are 250 m, while those of blue and green ones are 500 m.

We surveyed the MODIS images observed during the summers (late June to early September) in 2003 to 2005 and found the urban clouds in 29 images observed on 22 days. Number of the days when urban clouds were observed are consistent with the difference in the probability of cloud cover between the urban and the rural areas, which has been reported to be about 10 % in calm and clear days in Section 2.

In order to reveal the time variation of the urban clouds, photographic observations that were described in Section 3 were conducted at the point shown by an inverted triangle in the region A in Fig. 4.1. We focused on the clouds over the urban area indicated by "b" in Fig.4.1, as well as those above the rural area located to the west of the urban area. The observations were conducted on the selected fifty-four days during summer in 2003, 2004, and 2005.

4.2. Results

4.2.1. Horizontal cloud distribution in CTRL

Figure 4.3a shows the horizontal distribution of small cumulus clouds at 1030 LST simulated in CTRL. In the figure, light brown, dark green and light blue indicate the urban areas, the rural areas and the water surfaces, respectively. White areas indicate cloud cover. We are going to discuss cloud distribution, but amount of cloud water here.

Small clouds systematically distribute above EUAs in Region A, forming cloud lines above each EUAs. In particular, a cloud line is prominent above EUA-b. On the other hand, no cloud cell can be found in the rural area between EUA-a and EUA-b. Few clouds are distributed not only above the other rural areas near EUAs, but also in the northern half of the entire domain except for mountains. Small clouds scatter over inland of LUA, while no cloud is formed above the coastal areas around the Tokyo Bay in the LUA.

Figure 4.3b is a satellite image observed by Terra/MODIS at 1035 LST on a typical day, 4 August 2003. The data of the image is the same as Fig. 3.3a, but the domain is fitted to that of Fig. 4.3a. Dark gray, green and dark blue indicate the urban areas, the vegetated areas and the water surface, respectively. Urban and rural areas are corresponding to the lower and the higher NDVI areas shown in Fig. 2.3a, respectively. The vegetated areas roughly correspond to the rural areas in Fig. 4.3a. A numerous small clouds distributed above EUAs forming cloud lines similar to those of Fig.4.3a, except for above EUA-a. The size of observed cloud cell is much smaller than that of the simulated cloud cells. The reason is the coarse grid interval of the model.

The simulated cloud distribution has good similarity to that in the satellite images, particularly in the following characteristics: (1) cloud lines form above EUAs, (2) the cloud lines consist of small cloud cells, (3) clouds are sparse in the rural areas near EUAs, (4) clouds are randomly distribute inland of LUA, (5) clouds are sparse in the coastal areas.

The simulated cloud lines still consist of many cloud cells above EUAs at 1210 LST (Figure 4.4a). The cloud fraction has increased in EUAs, but few clouds are formed in the rural

areas. The clouds along the sea breeze front have shifted to near the northern boundary of LUA as the sea breeze penetrated inland. Figure 4.4b displays the satellite image of Aqua/MODIS observed at the same time as Fig. 4.4a that is about one hour and half later than that of Figure 4.3b. This figure also is the same as Fig. 3.3b, and the domain is fitted to Fig. 4.4a. Since the size of the cloud cells was enlarged, the cloud fraction increased above EUAs, particularly, the cloud line became wider and its density prominently increased above EUA-b.

Figure 4.5a-d shows the distribution of the small clouds on the hours between 0900 LST and 1300 LST in CTRL. Time evolution of the small clouds in CTRL is described as follows. At 0700 LST, the first small cloud formed in the mountain region located in north of the plain. Those clouds continuously existed till the sunset in the mountain areas. At around 0800 LST, small clouds form the coastal area in LUA, and then formed a cloud line above the sea breeze front. Shortly after that, small clouds appeared also in EUAs, and then they formed cloud lines along the areas. Contrast in cloud distributions between the urban areas and the adjacent rural areas became very sharp and then became stationary from 1000 LST to about 1200 LST. Figures. 4.5e-h indicate the distribution of small clouds on the hour in Case N00, which assumes no urban area in the sensitivity experiments described in Section 4.2.6. The clouds form systematically above EUAs in CTRL, in contrast, clouds randomly distribute in Case N00. These figures demonstrate that the urban effects suppressed cloud formation in the surrounding rural areas in CTRL.

The lifetime of the simulated cloud lines in EUAs is summarized in Table 4.1. The lifetime of the cloud line in EUA-b was the longest, which was about four hours, from 0850 LST to 1300 LST. The second longest one was formed above EUA-c, and it was about three hours. The shortest one was only thirty minutes formed in EUA-a. A lifetime of a cloud line above an EUA seems to depend on the size, the shape, and the geographical location of the EUA.

4.2.2. Time evolution of small clouds in CTRL

Figure 4.6a shows the evolutions of the simulated cloud fractions above the urban and the rural areas in Region A. The cloud fraction is defined as the percentage of the number of grid points covered by to the number of total grid points in the estimating area. The cloud fractions were estimated every 10 min in the urban and the rural areas in Region A, which includes 474 and 415 grid points, respectively.

At around 0800 LST, the cloud fraction begins to increase in the urban area although that in the rural stays almost zero. After that, the urban cloud fraction increases steeply until 1300 LST with some fluctuation. The rural cloud fraction eventually begins to increase at around 1100 LST, while it is much lower than that of the urban until 1300 LST. After the sea breeze covers the entire region (1300 LST), the cloud fractions in both areas begin to decrease narrowing down the difference in cloud fraction between the urban and the rural areas.

4.2.3. Vertical structures

In the urban areas, strong ascending flows are dominated in the mixed layer before noon. Figure 4.7 shows vertical velocity at the height of 439 m at the sampling points in urban (the solid line) and rural (the dashed line) shown in Fig. 4.1, respectively. A strong ascending flow intermittently appears in the urban area, while a mild downward flow prevails stationary in the rural areas near the urban areas. Figure 4.8 indicates the horizontal distribution of w-component at the same level. Red and green indicate upward and downward flows, respectively. Dark color shows a stronger flow. Light-gray boxes indicate urban grid points. Strong ascending flows distribute in a part of the urban areas. Some of them are lined in rows along the long urban areas, but especially in EUA-b and the inland of LUA, strong and weak ascending flows coexist in intricate pattern. Those ascending flows seem to be thermals rather than upward winds of horizontal circulations. On the other hand, the downward flows prevail in the entire rural areas. The downward flows seem to be the compensating downward flows induced by the ascending

flows over the urban areas.

Figure 4.9 shows the vertical cross section of potential temperature with cloud water contents at 1020 LST. Warm colors indicate higher potential temperatures. White indicates the presence of clouds. Light-brown and light-green boxes just above x-axis are urban and rural grid points, respectively. The cross section shown by the dashed-dotted line in Fig. 4.1 is across EUA-a, -b, and -c. Fig. 4.10 shows that of mixing ratio at 1020 LST. Dark-blue indicates higher mixing ratio. Absolute unstable condition in the simulated atmosphere is limited in the urban surface layer (Fig. 4.9), while potential temperature and specific humidity are almost vertically uniform in the mixed layer, so that relative humidity becomes higher with altitude.

Figures 4.9 and 4.10 show also the composite of horizontal wind along the cross section and w-component, which is multiplied by 20. The small cumulus clouds form at the top of the ascending flows above the urban areas. The ascending flows are likely to be thermals in the mixed layer, although the horizontal sizes of the simulated ones are much larger than those in the real atmosphere. The mixed heights at 1030 LST were 1340 m and 1070 m at the urban and rural sampling points shown by the black and white circles in Fig. 4.1, respectively. The urban mixed layer is higher than that the rural one, thus the ascending flows can easily reach the lifting condensation level (LCL). In contrast, the downward flows suppress the height of the mixed layer in the rural areas, so that relative humidity near the top of mixed layer tends to be lower than that of the urban atmosphere.

4.2.4. Wind velocity

The solid line in Figure 4.6c shows simulated vector mean wind velocity at the lowest level (14 m) in Region A. Mean velocity is lower than 2.0 m/s before 1200 LST until when contrast of the cloud fraction is very sharp between urban and rural. Wind direction ranges in easterly to southeasterly. Since the region is covered by the sea breeze after 1200 LST, wind

velocity becomes higher than 2 m/s, and contrast of cloud fraction begins to decrease with dissipation of the urban clouds. Figure 4.11 shows the horizontal wind velocity at the lowest layer at 1020 LST in CTRL. The sea breeze from Tokyo Bay prevails in two-thirds of the bay side of LUA, while the inhomogeneous winds prevail in Region A and the inland of LUA. In Region A, wind velocity in the rural areas is weaker than that in the urban areas. The center of divergence of the sea breeze is over Tokyo Bay as noted by Kimura and Takahashi (1991). The sea breeze front exists near the northern edge of LUA at this time, while the front penetrate deeper into inland, around 36.0° N, at 1500 LST.

4.2.5. Comparison with the ground-based photographic observation

The evolution of the small clouds in CTRL is consistent with that of the ground-based photographic observation described in Section 3.

The onset time of the urban clouds in CTRL is around 0800 LST and the dissipation time is early in the afternoon. The duration of the simulated clouds is about six hours, although the dissipation time in the model was unclear due to the effect of the sea breeze. They agree well with the results of the photographic observation, in which the onset time of the urban clouds was between 0800 LST and 1130 LST, and the dissipation time was between 1300 LST and 1700 LST as shown in Section 3.2.2.

4.2.6. Sensitivity experiments in thermal effect

Sensitivity experiments were conducted to estimate the necessary minimum heat contrast between urban and rural areas. The thermal effect of the contrast between urban and rural areas is controlled by the soil moisture at the urban grid points in the experiments. The soil moisture is kept to be the same value in the rural area. Thus, smaller moisture availability in the urban area leads to stronger thermal contrast. In CTRL, the soil moisture in the urban grid points is assumed to be 65 % of that at the rural grid points. In experiments, those of the urban grid points are set to

75%, 85% and 100% for Cases U75, U85 and N00 respectively. Case N00 does not assume any urban area. Sensible heat flux will decrease with soil moisture in the urban area.

The results of the sensitivity tests are summarized in Table 4.2. Urban and rural sensible heat fluxes are defined as averages in the entire urban and rural areas of the domain, respectively. An index for the heat contrast can be defined as the ratio of the maximum sensible heat fluxes between urban and rural areas. The index ratio of CTRL is 6.9, while the maximum sensible heat fluxes are 297 W/m² at 1240 LST and 43 W/m² at 1110 LST in the urban and the rural areas, respectively (see Fig. 4.6b). After the onset of the urban clouds, the heat flux ratio exceeded 5.5 until cloud dissipation time. Table 4.2 also shows the onset time of the cloud and the sensible heat flux (130 W/m²) in urban areas at the onset.

Figure 4.12 shows the cloud fraction, the sensible heat flux, and the wind velocity in Case U75. The index ratio of Case U75 is 4.3. The evolution of the urban clouds is almost the same as that in CTRL except for 30 minutes delayed onset of the urban cloud. Although a few clouds appear in rural areas from 0930 LST to 1030 LST, clouds are almost suppressed in the rural areas before 1100 LST. The forcing of the cloud suppression still exists, although the forcing seems to be slightly weaker than that of CTRL. The maximum sensible heat fluxes in the urban and the rural areas are 199 W/m² (1300 LST) and 46 W/m² (1110 LST), respectively. The wind velocity is slightly stronger than that in CTRL.

The index ratio is 1.9 in Case U85, which is much lower than that in CTRL. The evolution of clouds is shown in Fig. 4.13a with those of sensible heat fluxes (Fig. 4.13b) and wind velocities (Fig. 4.13c). The onset times of a small cloud in the urban and the rural areas are almost the same. The evolution of clouds in the rural areas is synchronized with that in the urban areas during 0900 LST to 1030 LST. Cloud fraction in rural areas is slightly lower than that in the urban area after 1030 LST. The cloud suppression in the rural areas is very weak in this case. These results suggest that the ratio of the maximum heat flux should be at least larger than 1.9 in order to form a clear contrast in cloud fraction between the urban and the rural areas.

In addition, mean levels of the cloud base in the urban area simulated in Case U75 and U85 are lower than 12% and 20%, respectively, of that in CTRL at 1100 LST.

Small clouds also generate in Case N00, which assumes uniform surface condition without urban areas (Fig. 4.5e-h). Cloud distribution is unstructured except for clouds caused by sea breeze fronts, a wind convergence line extending from Miura Peninsula and orography. Small clouds form independently of the surface conditions in the areas farther inland of the sea breeze fronts. These clouds are not stationary in contrast with those in CTRL. Figure 4.14a indicates the evolution of the cloud fraction in Case N00. The solid and the dashed lines indicate the cloud fractions of the areas, which correspond to the urban and the rural areas in CTRL, respectively. The maximum sensible heat flux in Case N00 is 49 W/m² at 1130 LST (Fig. 4.14b); the wind direction is more southerly than that in CTRL (Fig. 4.14c).

4.2.7. Sensitivity for wind field

Cloud formation is affected not only by sensible heat flux but also by the ambient winds. Additional sensitivity tests were conducted focusing on the ambient wind velocity. Each test assumes different initial and boundary conditions of wind. Wind velocities below the level of 900 hPa were assumed to be 1 m/s (CTRL), 2 m/s (Case Uw2) and 3 m/s (Case Uw3). Figures 4.15a-d and 4.15e-h indicate the horizontal distribution of small clouds from 1000 LST to 1300 LST in Cases Uw2 and Uw3, respectively. Small clouds tend to form in some rural areas located downwind of the urban areas especially in the morning. Figures 4.16a and 4.17a indicate the time evolution of cloud fraction in Cases Uw2 and Uw3, respectively. As a result of downwind clouds, the difference between of cloud fractions in the urban and the rural areas became smaller in Cases Uw2 and Uw3 than that in CTRL in spite of the same level of sensible heat fluxes (Figs. 4.16b and 4.17b). The time of the maximum cloud fraction in the urban areas becomes earlier than that in CTRL. Especially in Case Uw3, clouds completely dissipate after around 1400 LST,

which is four hours earlier than CTRL. The times of the wind speed over 2 m/s in these cases are faster than that in CTRL (Figs. 4.16c and 4.17c).

4.3. Discussion

4.3.1 Maximum sensible heat flux of urban areas in summer

We have almost no information on observational values of sensible heat fluxes in the urban areas where we are studying. The maximum sensible heat flux in urban areas of CTRL, 297 W/m², can be compared with those of other studies of urban canopy models and also with urban canopy observations at a few points in mid-latitudes. Kusaka et al. (2001) made a comparison between three types of urban models, which are a multi-layer urban model, a single-layer urban canopy model, and a slab model. The last one is the almost same as the simple urban expression in the present study. Maximum sensible heat fluxes of the three models range from about 220 W/m² to about 250 W/m², which lie between those of CTRL and Case U75. Kusaka et al. (2001) stated that critical difference of sensible heat fluxes between the multiple layers model and the slab model exists in the nighttime. In other words, sensible heat fluxes given by the slab model assuming in the present study are not largely different from the values estimated by other methods in the daytime. Rotach et al. (2005) reported that maximum sensible heat fluxes observed in urban areas in midsummer range from about 300 W/m² to 400 W/m². The observation was carried out as a part of the Basel UrBan Boundary Layer Experiment (BUBBLE) in Switzerland. These values are almost equal to or slightly higher than that in CTRL. The observation by Kanda et al. (1997) showed that the sensible heat flux in a high-density area of Tokyo was recorded between about 150 W/m² and 250 W/m² around noon on a sample day. In addition, they also indicated that the latent heat flux from cooling systems installed in office buildings is comparable to the sensible heat flux in the area.

On the paddy fields in the rural area, daily maximum sensible heat flux was about 50

W/m² by Bowen ratio method on 4 Aug 2006, which was a typical clear calm day. The observation site is located in the northeast rural area in Region A. The simulated flux shown in Table 2 almost agrees with this value. Thus we can conclude that the value of the maximum sensible heat flux in CTRL is reasonable and the sensitivity tests cover most likely conditions around the domain during daytime in summer.

4.3.2. Thermal or horizontal circulation?

Generally, fair-weather clouds are often formed in a clear day as the result of penetration of the thermals into the stable layer beyond the LCL above the mixed layer. These clouds usually onset in the early stage of the development of the mixed layer. The thermals rise by some trigger mechanism such as orography or surface thermal discontinuities. Orography is one of the strongest triggers, which often induces the first cumulus cloud, as shown by CTRL in which the first cloud formed over the mountains. Obviously, the thermal contrast between urban and rural has enough capacity to be the triggers.

The observed cloud lines consist of many small cloud cells. These small cloud cells seem to be the cumulus clouds formed by the thermals, which are triggered by the thermal anomaly in urban area. Onset time of the observed clouds does not conflict with this viewpoint. Furthermore, many small cumulus clouds also randomly formed in the inland of Tokyo in Fig. 4.3b. They seem to be the Bènard-cell type cumulus clouds. Figures 4.18a and 4.18b show the distributions of sensible heat flux and latent heat flux at 1030 LST, respectively. The fluxes in LUA and EUAs are almost the same level, so that the absolute unstable condition as shown in Fig. 4.9 is formed in the surface layer of both areas. Thus, it is reasonable for us to think the factor of small cloud formation in EUAs is the same as that in LUA.

In the mixed layer over uniform land surface, there are large numbers of weak inter-thermal downdrafts, which are much wider than the thermal updrafts (Stull, 1988). These

downdrafts are forced to be in the rural areas, because of prominent thermals in the urban area. This mechanism could be a reason of the simulated downward flow and the cloud suppression in the rural areas.

Another aspect of the updrafts inducing cloud forming is the mechanism of a horizontal convection, which explains most of the thermally induced mesoscale circulations, such as sea/land breezes, mountain/valley winds and urban heat island circulations (UHIC here after). Horizontal convection does not always need an absolute unstable condition but the horizontal contrast of atmospheric temperature. Updrafts can be formed by the UHIC between EUAs and rural. Avissar and Liu (1996) stated that upward motion of mesoscale circulations generated by landscape heterogeneities is stronger than the thermal cells, and that clouds formed over dry-soil areas can be explained by these circulations. The horizontal convection explains well the shape of the observed clouds distribution over EUAs, i.e., these are line-shaped with narrower width than that of EUAs especially in the early stage as shown in Fig. 4.3b. The cloud suppression in the rural areas corresponds to the downward flows as a part of the horizontal circulation. However, this mechanism cannot account for the small cell structure of the cloud lines.

It is quite interesting question whether the urban cloud is formed by a vertical convection or a horizontal convection. The former includes thermals in the ML, while the letter includes UHICs. However, we cannot answer this question because of the coarse resolution of the numerical model as mentioned above. This model cannot explicitly simulate microscale phenomena like thermals. The simulated convection is quite ambiguous and may have both aspects. However, this problem will not be serious for the cloud line formation, because updraft of the mesoscale circulations are expected to be stronger than that of thermals as discussed in details by Avissar and Liu (1996).

4.3.3 Cloud suppression in the sea breeze area

Fair-weather clouds are strongly suppressed in the area covered by a sea breeze even in the urban area. In CTRL shown in Fig 4.3a, the suppressed area is covered by two sea breezes from Tokyo Bay and Sagami bay. Sea breeze fronts are located inland boundary of the cloud-suppressed area, where cloudiness is slightly higher than the outer regions of the suppressed area. The satellite images (Fig. 4.3b) also shows quite similar cloud distribution around the area which is likely to be covered by a sea breeze, although the clouds are prominently intensified along the sea breeze fronts, particularly at 1210 LST (Figure 4.4b). Cumulus clouds and even deep convections are well known to be frequently observed along the sea breeze fronts. The suppression of clouds is often observed in the coastal urban area when the urban cloud lines are observed. Sea breeze should provide unsuitable conditions for forming of the fair-weather clouds. The mechanism of the cloud suppression there seems to be different from the suppression in the rural areas of Region A. One of the reasons for the suppression is strong horizontal velocity of the sea breeze, which can destroy the small convection systems. The sensitivity test for the ambient wind velocity indicated that the clouds became difficult to form when velocity of the southerly wind is larger than 4 m/s. The sea breezes provide such conditions and suppress the clouds. Another reason is a downdraft behind the sea breeze, which covers most part of the sea breeze area except for near the sea breeze front.

4.4. Summary

Small cumulus clouds formed above urban areas along railroad lines were simulated by the numerical model and elucidated its mechanisms. The distribution and the time evolution of those simulated clouds were agreed well with those of the satellite images and the ground-based photographic observation on typical days. The model indicated that the small clouds are not only enhanced in urban areas but also suppressed in surrounding rural areas. The distribution of small

clouds is quite sensitive to the thermal contrast between urban and rural. When the ratio of sensible heat flux between them is about seven, the contrast between the cloud formation in the urban areas and the suppression in the rural areas is very clear. The small clouds are formed only in urban areas but rare in rural areas, because urban effects on cloud suppression in rural area is predominant. The contrast of cloud fraction between urban and rural gradually decreases with the reduction of the thermal contrast. The contrast of cloud fraction is weakened but is still clear when the ratio of a sensible heat flux is 4.3. When the ratio is 1.9, the cloud suppression in rural areas disappears.

The mechanism of cloud contrast is as follows: 1) Thermals form in the mixed layer above the land surface. 2) Because of the larger sensible heat flux, the mixed layer tends to be higher in the urban area; thus, thermals reach the lifting condensation level more easily than they do in the rural area. 3) The wide compensating downdrafts of the strong urban thermals cover the entire rural area and suppress thermals and clouds there.

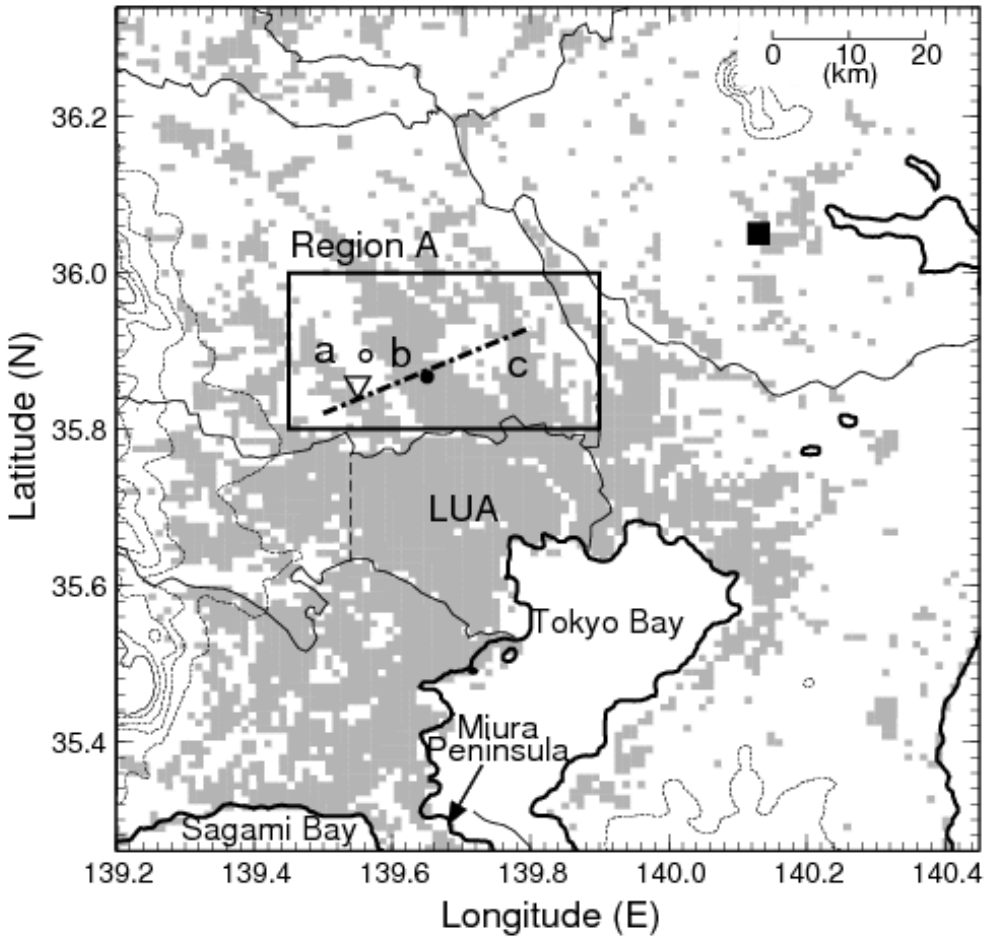

Figure 4.1: Domain of the fine grid system. Shading indicates the urban grid points. The rectangle indicates Region A. The lowercased letters a, b, and c in Region A indicate extending urban areas (EUAs). The inverted triangle, the black and the white circles in Region A indicate the photographic observation site, the urban and rural w-component sampling points, respectively. The dashed-dotted line indicates the cross section shown in Figs. 4.9 and 4.10. The black square indicates the Tateno sounding station. The thin solid lines indicate prefecture borders. The area enclosed by thin solid lines with a thin broken line indicates the large and dense urban area (LUA). The dotted line indicates a contour of 100 m intervals.

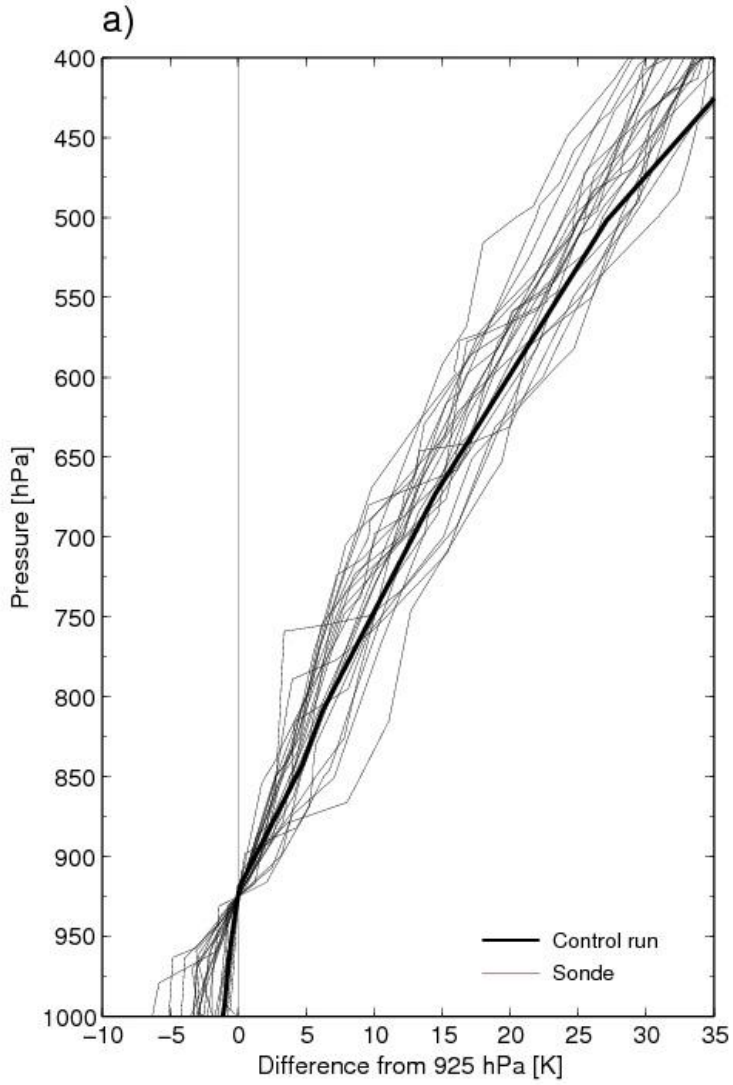

Figure 4.2: (a) Vertical profile of potential temperature as the difference from that at 925 hPa on the urban cloud days. The thin lines indicate those of Tateno station at 09 LST (00 UTC) on urban cloud days and the thick lines indicate those assumed in the model as the initial conditions.

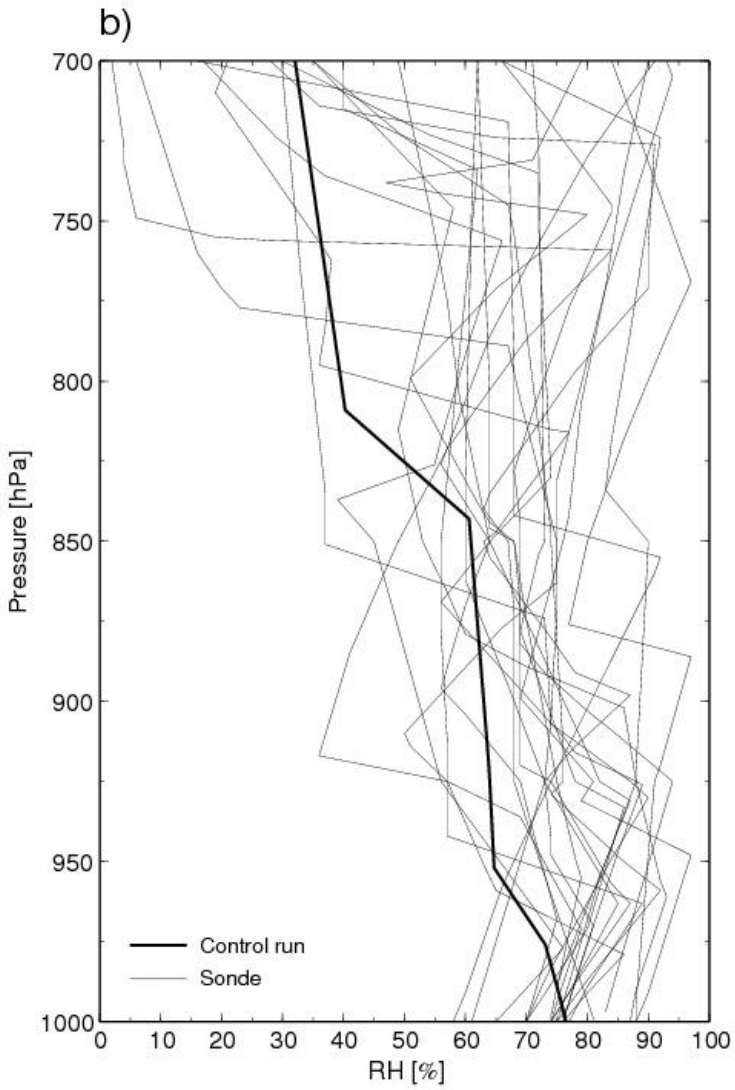

Figure 4.2: Continued. (b) Vertical profile of relative humidity.

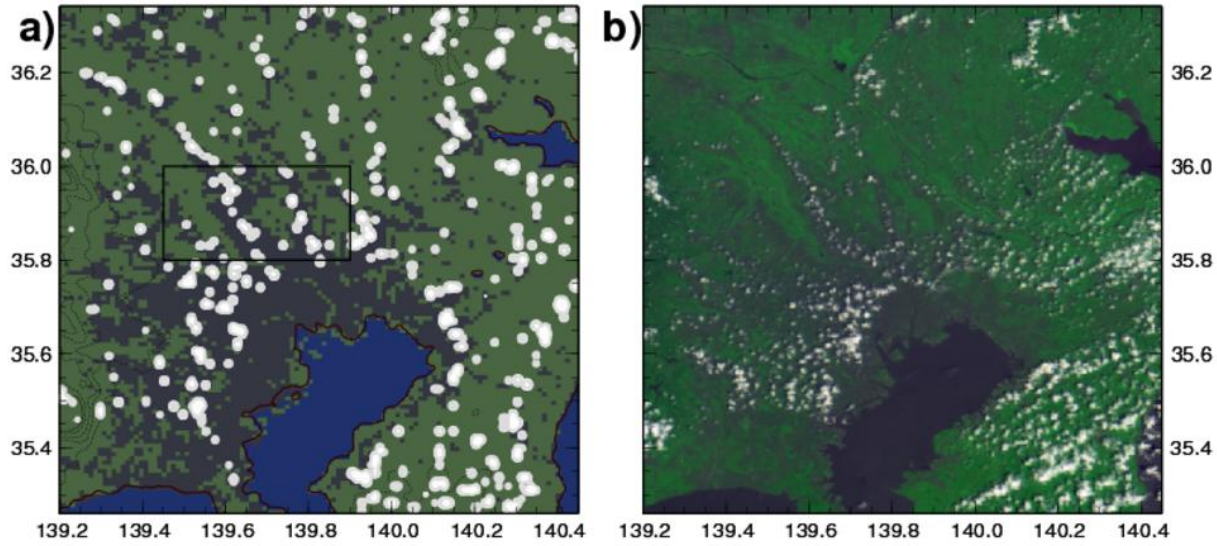

Figure 4.3: (a) The horizontal distribution of small cumulus clouds at 1030 LST simulated in the control run. The white areas indicate clouds. Dark-gray, dark-green, and blue indicate urban areas, rural areas, and water surfaces, respectively. (b) The satellite image observed by MODIS at 1035 LST on a typical day, 4 August 2003 (The same shot as Fig. 3.3a, except for the domain).

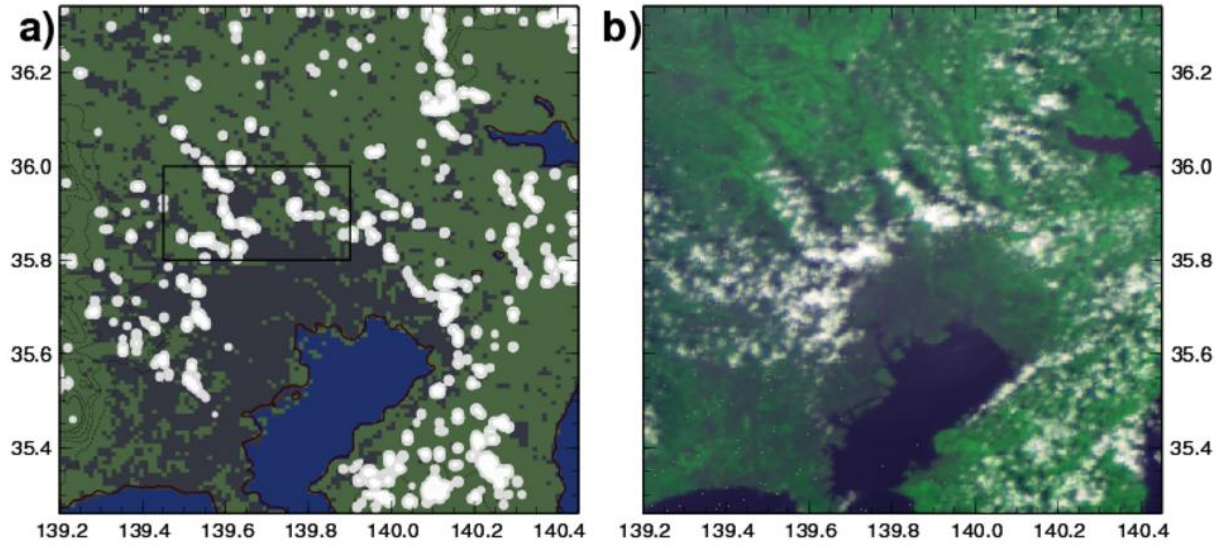

Figure 4.4: Same as Fig. 4.3 but for the time (a) 1210 LST and (b) 1210 LST (The same shot as Fig. 3.3b, except for the domain)

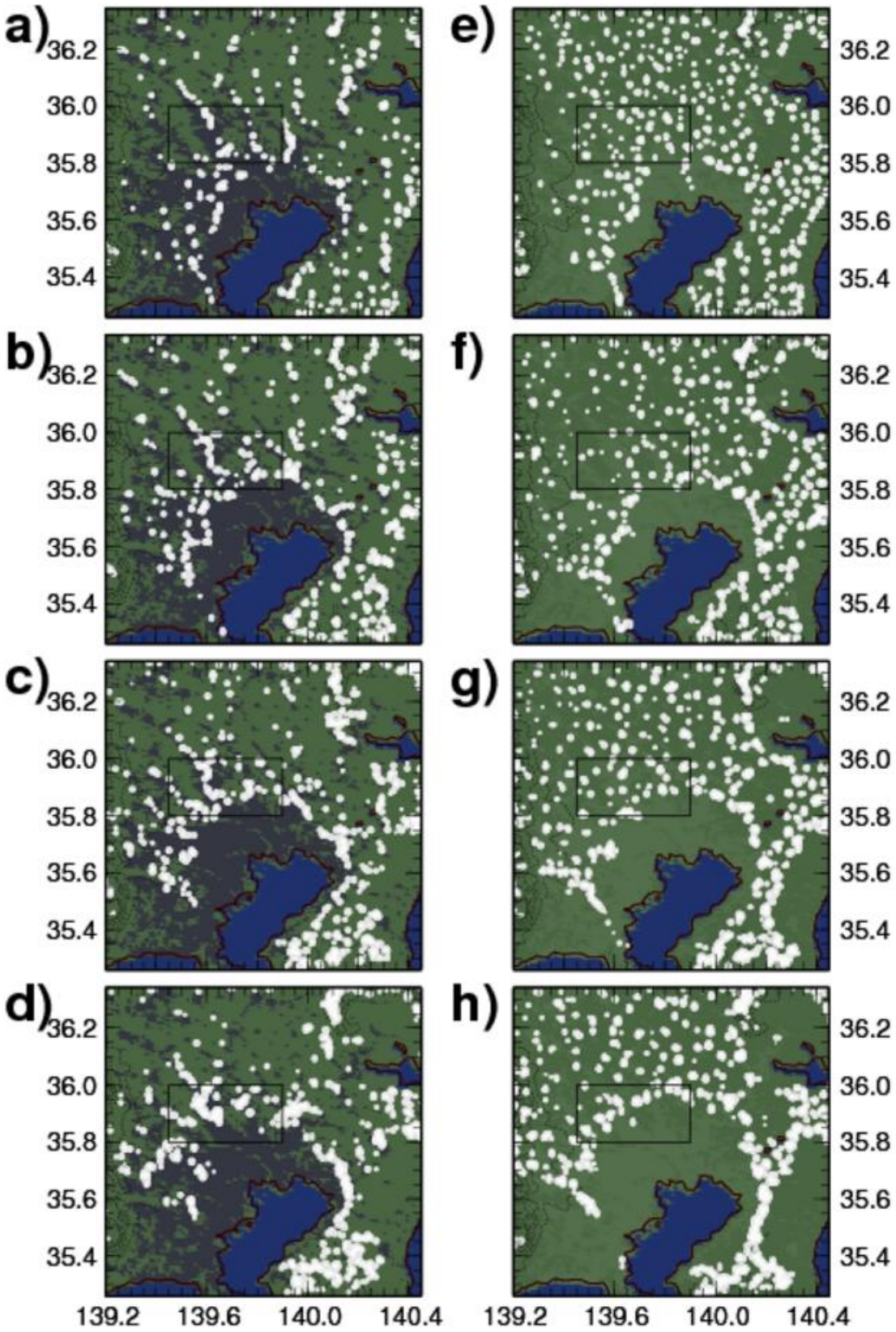

Fig. 4.5. Same as Fig.4.3a except for time (a) 1000 LST; (b) 1100 LST; (c) 1200 LST; (d) 1300 LST, and except for Case N00 and time (e) 1000 LST; (f) 1100 LST; (g) 1200 LST; (h) 1300 LST, respectively.

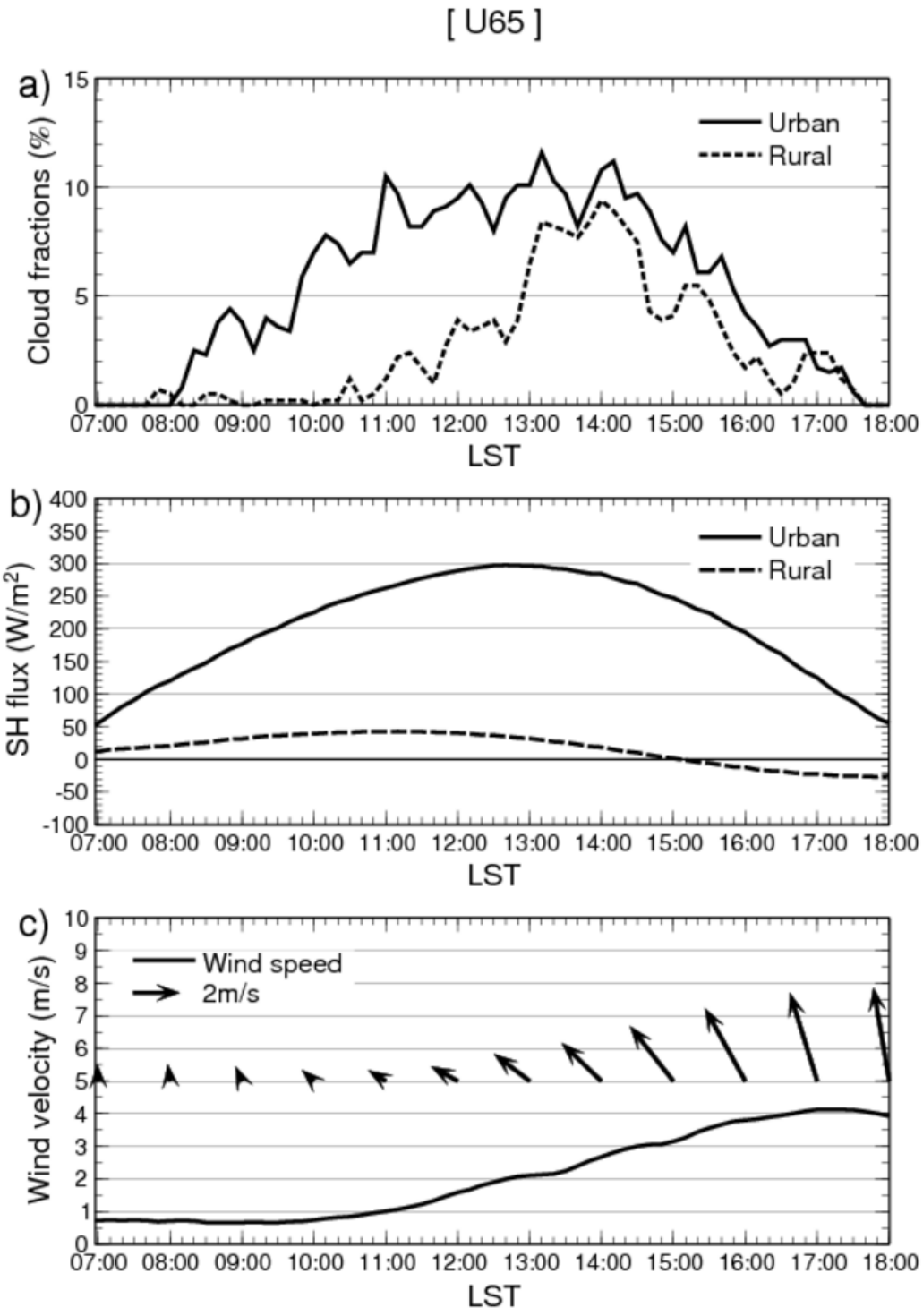

Fig. 4.6: The time evolution of (a) Cloud fraction, (b) The sensible heat fluxes (SHs), (c) The mean wind velocity in Region A. Solid lines and broken lines in (a) and (b) indicate the urban grid points and the rural grid points in CTRL, respectively. The solid line in (c) indicate the vector mean wind velocity.

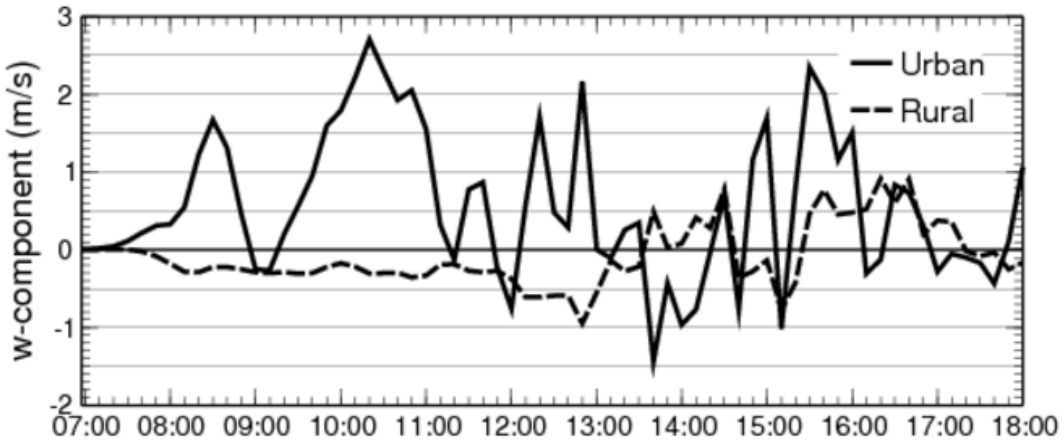

Fig. 4.7: W-components of the urban and the rural sampling point at the height of 439 m. The solid and the dashed lines indicate the urban and the rural grid points, respectively. The sampling points are shown in Fig. 4.1.

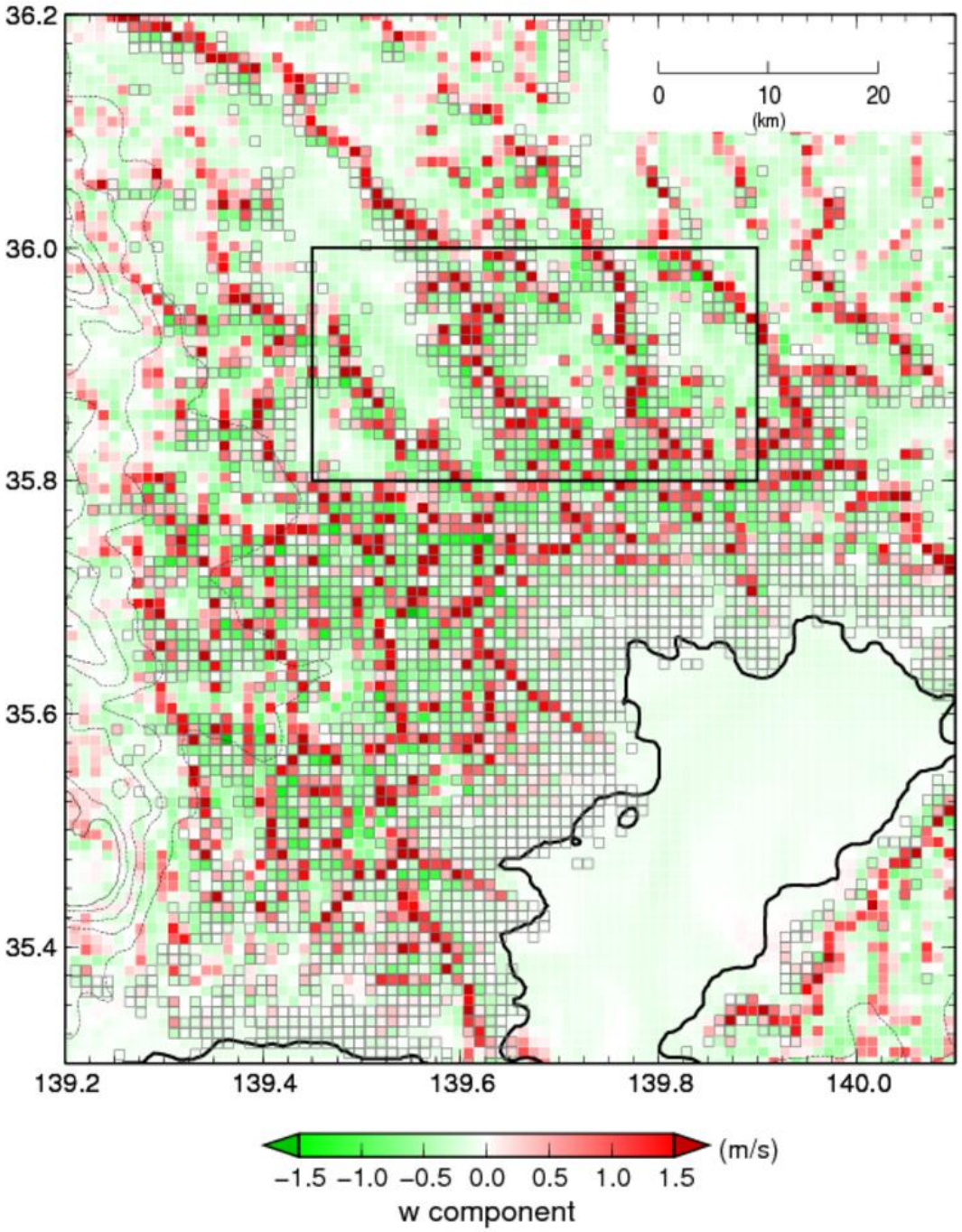

Fig. 4.8: The horizontal distribution of w-component at the height of 439 m at 1020 LST. Red and green indicate upward and downward flows, respectively. The rectangle indicates Region A.

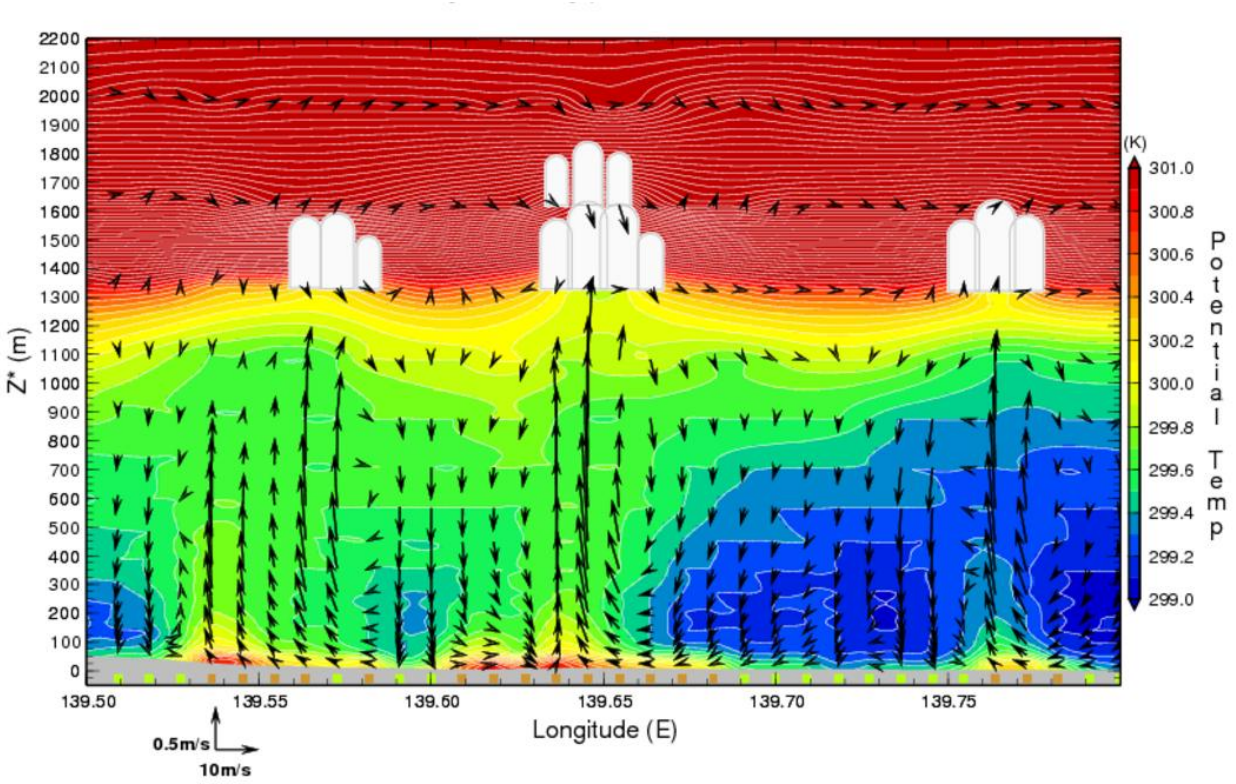

Figure 4.9: The longitudinal cross section of vertical structure of the potential temperature and winds at 1020 LST in Region A of CTRL. Color contours indicate the potential temperature. The scale of w-component is 20 times larger than the u-component. White indicates cloud of each model layers. Colors of under 0 m indicate land-use; brown and green indicate the urban areas and the rural areas, respectively. The cross section is shown in Fig. 4.1.

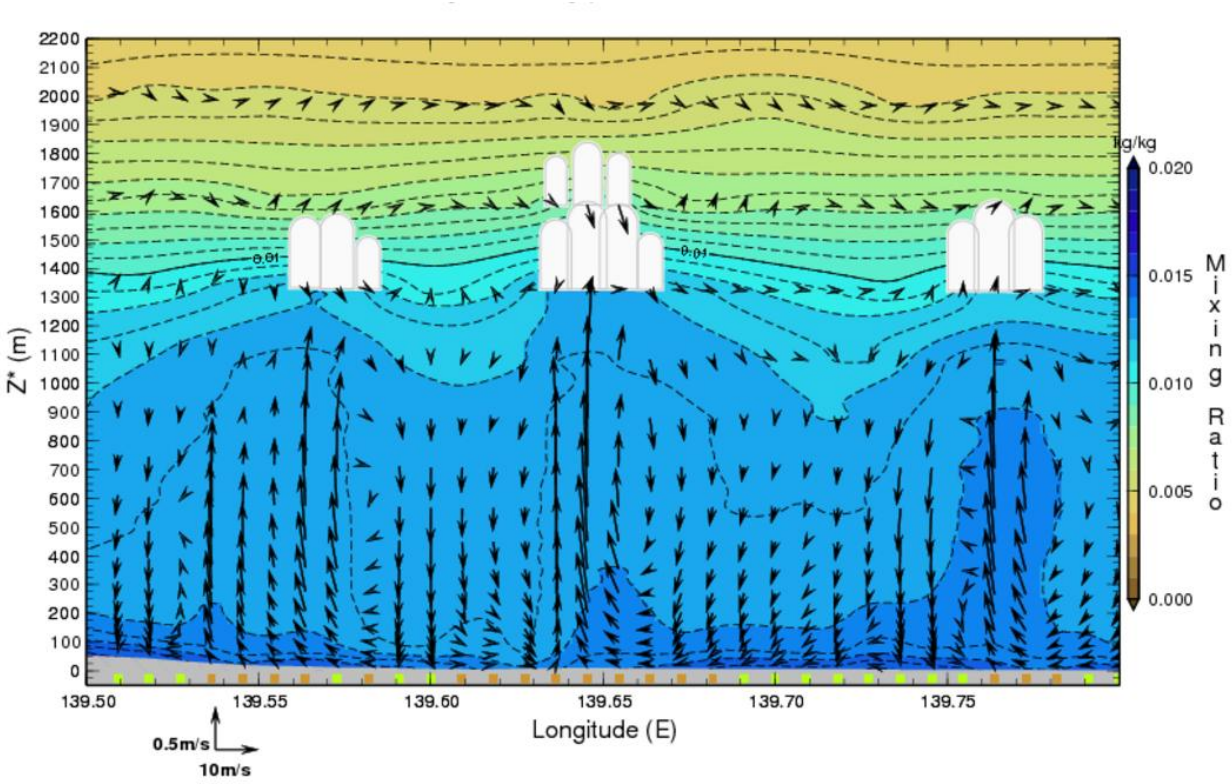

Figure 4.10: Same as Fig 4.9 except for the mixing ratio.

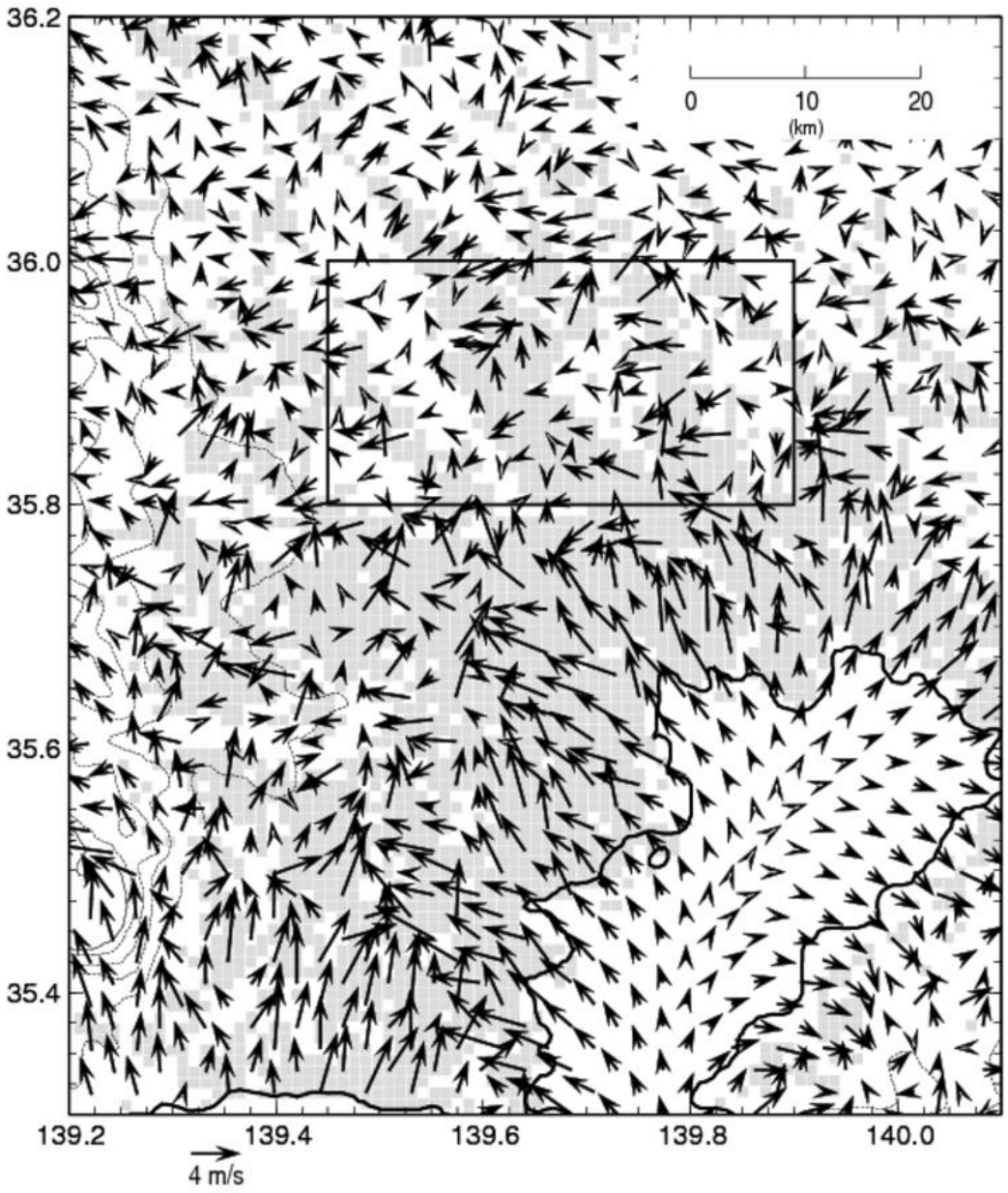

Figure. 4.11: The wind field of the lowest layer (14 m) at 1020 LST in CTRL. The rectangle indicates Region A.

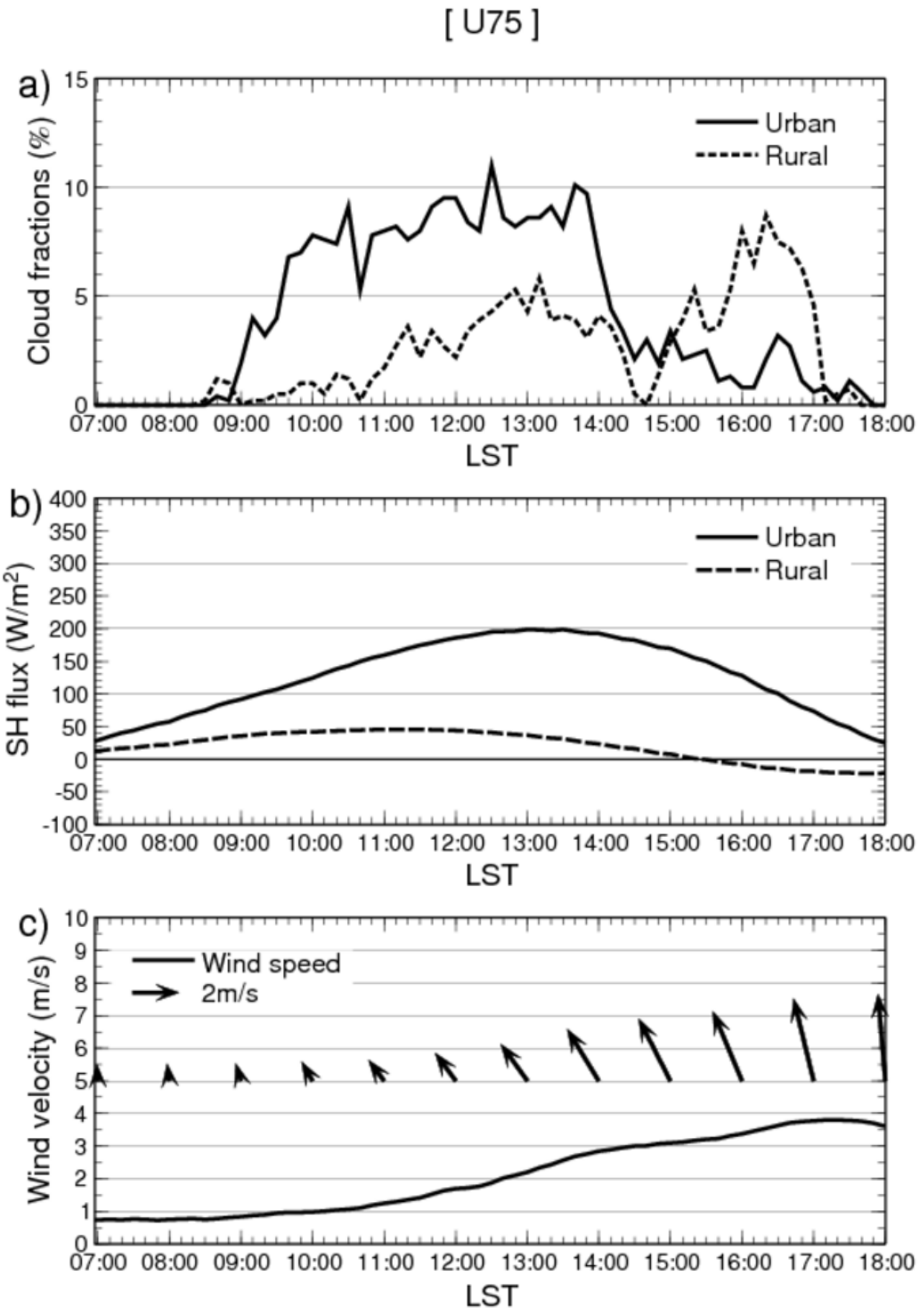

Figure. 4.12: Same as Fig. 4.6 but for Case U75.

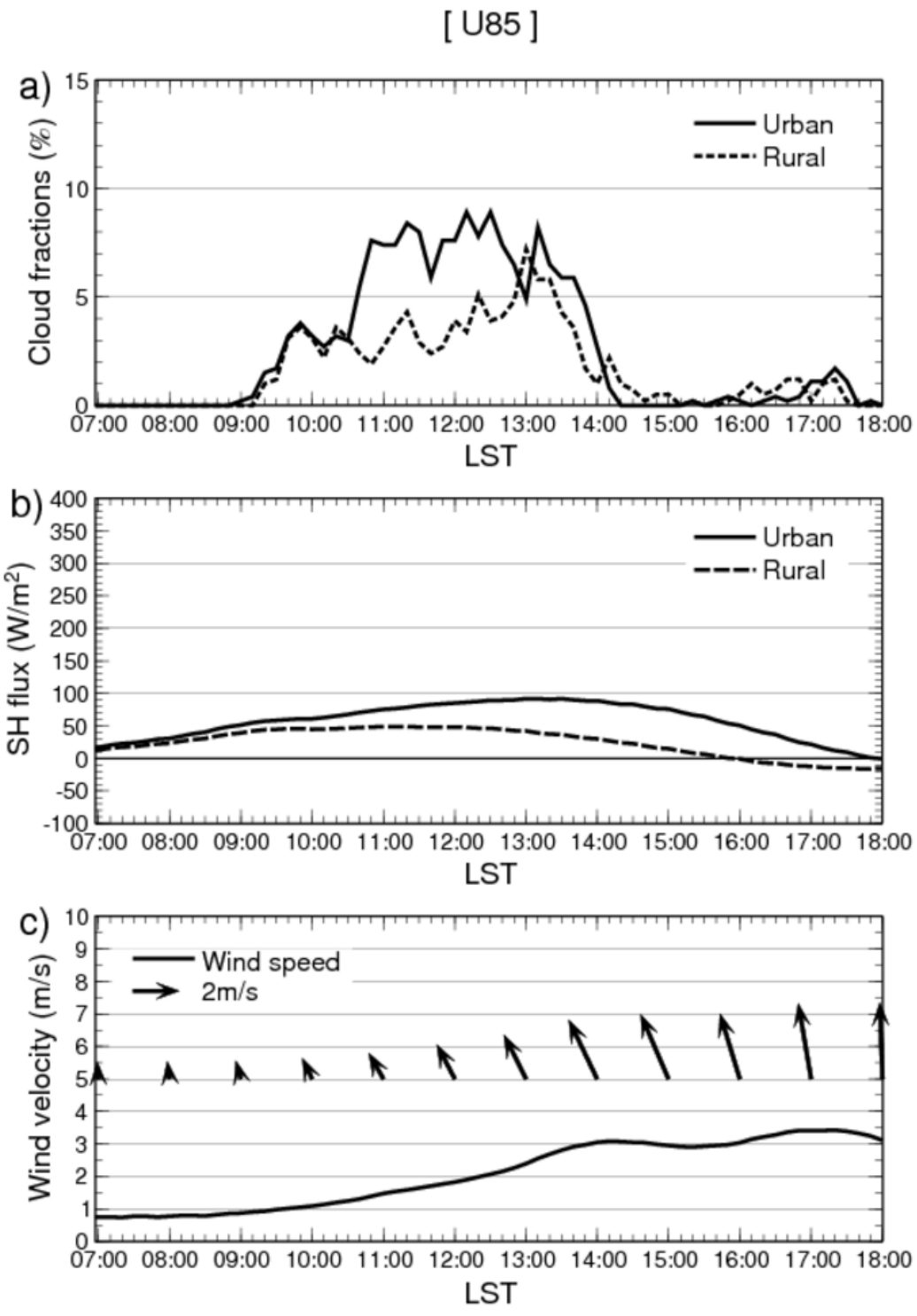

Figure 4.13: Same as Fig. 4.6 but for Case U85.

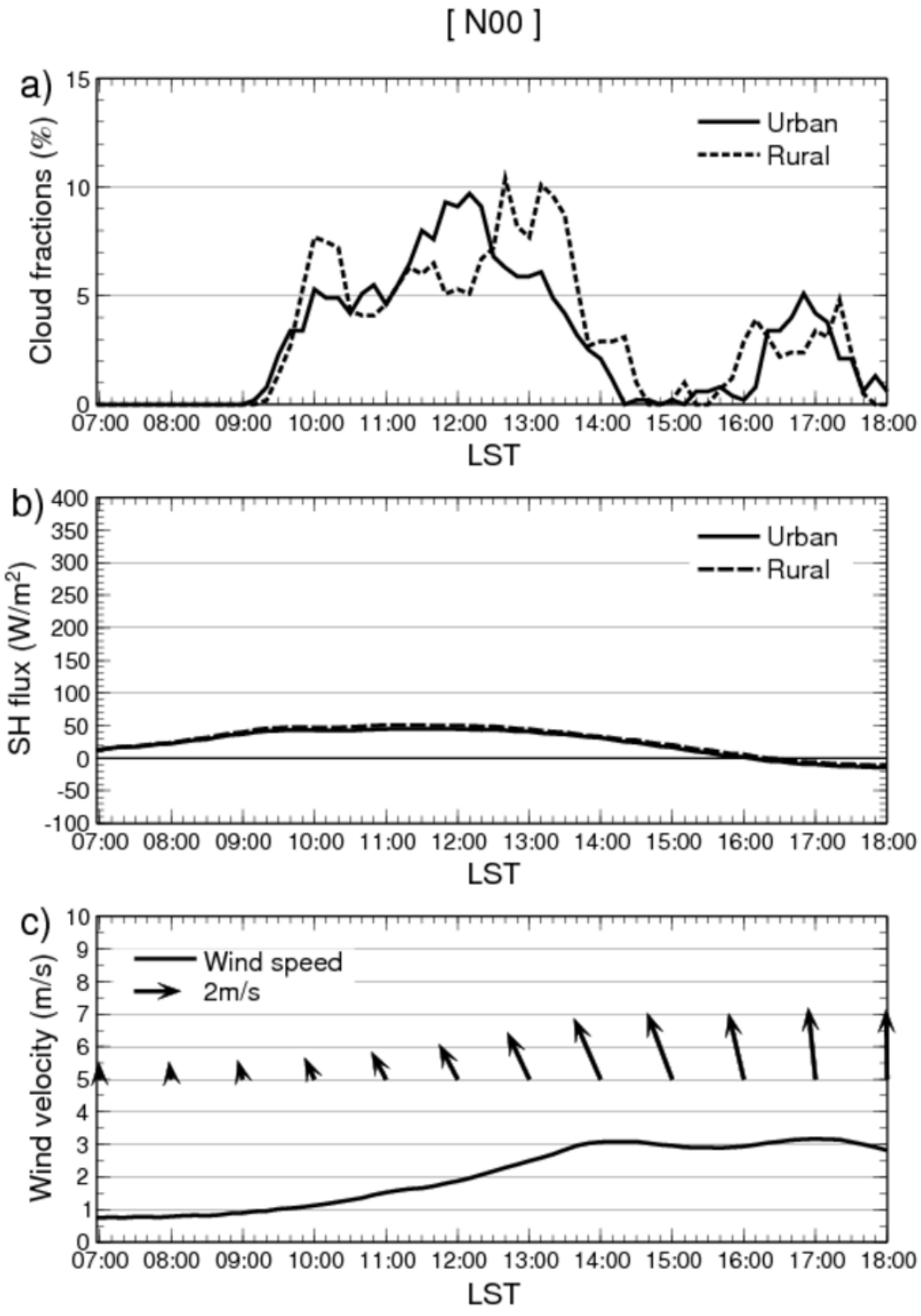

Figure 4.14: Same as Fig. 4.6 but for Case N00 (assumed no urban area). The solid and the dashed lines indicate the cloud fractions of the areas, which correspond to the urban and the rural areas in CTRL, respectively.

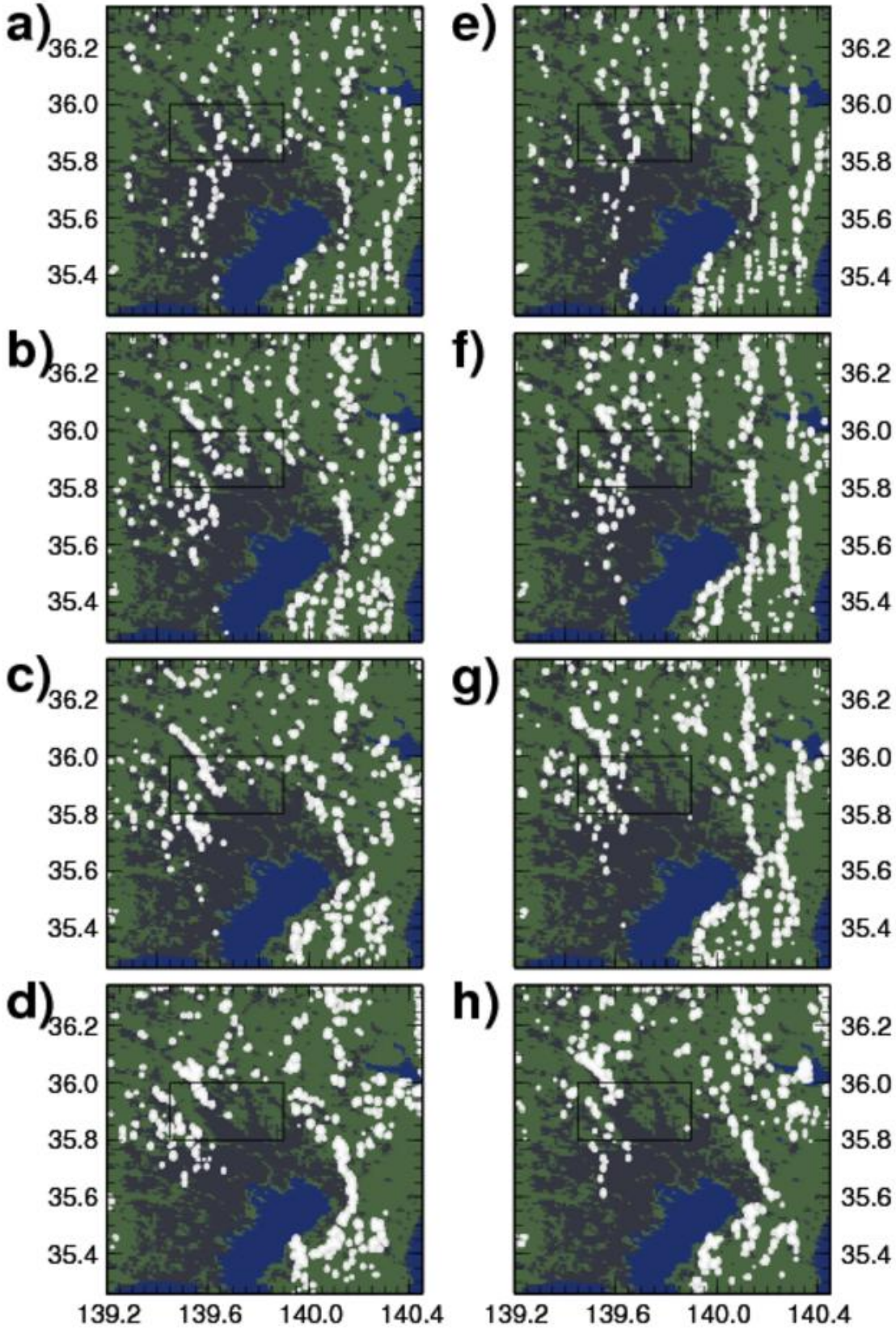

Fig. 4.15. Same as Fig.4.5 except that (a)-(d) are for Case Uw2 and (e)-(h) for Case Uw3.

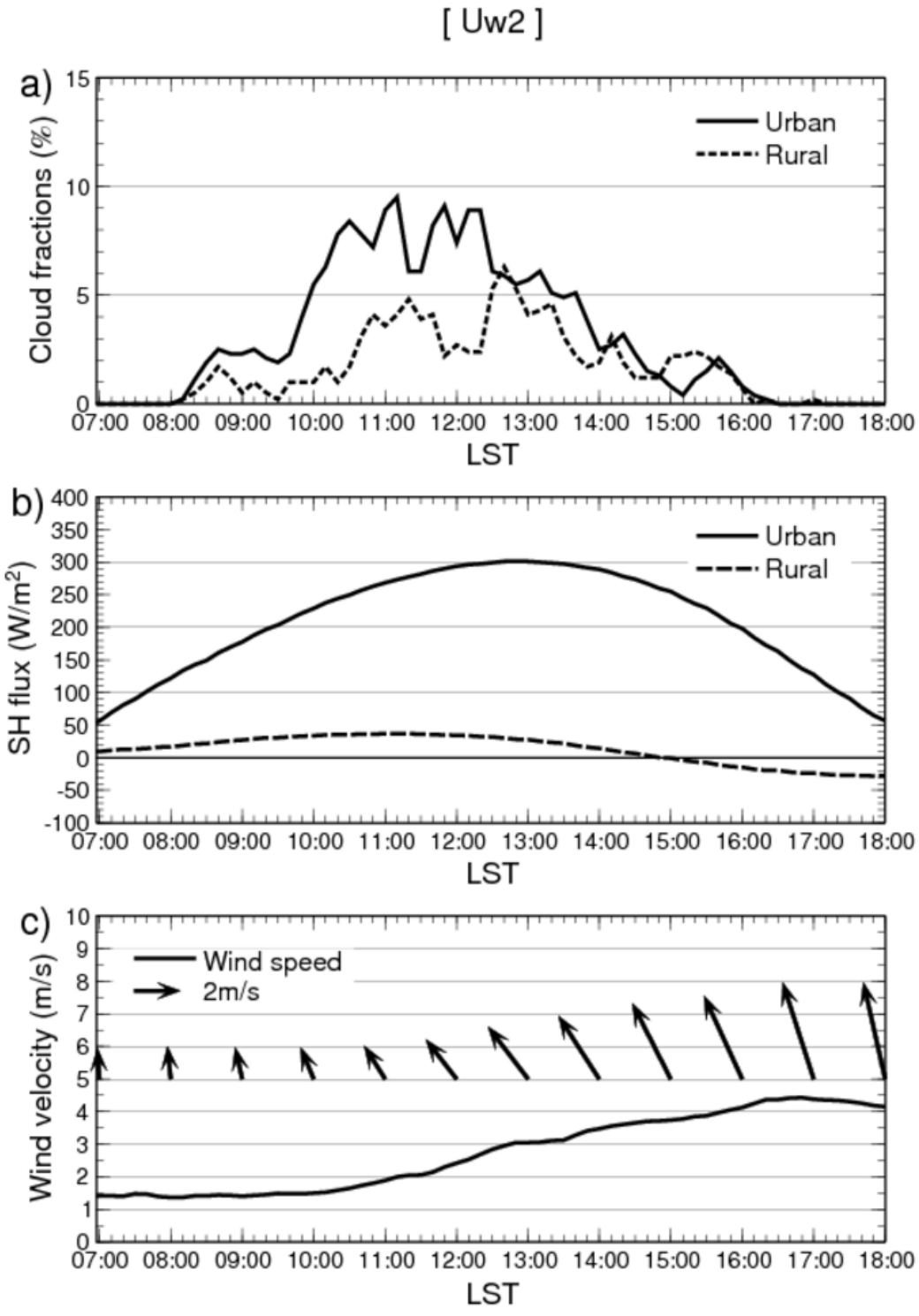

Figure 4.16: Same as Fig. 4.6 but for Case Uw2.

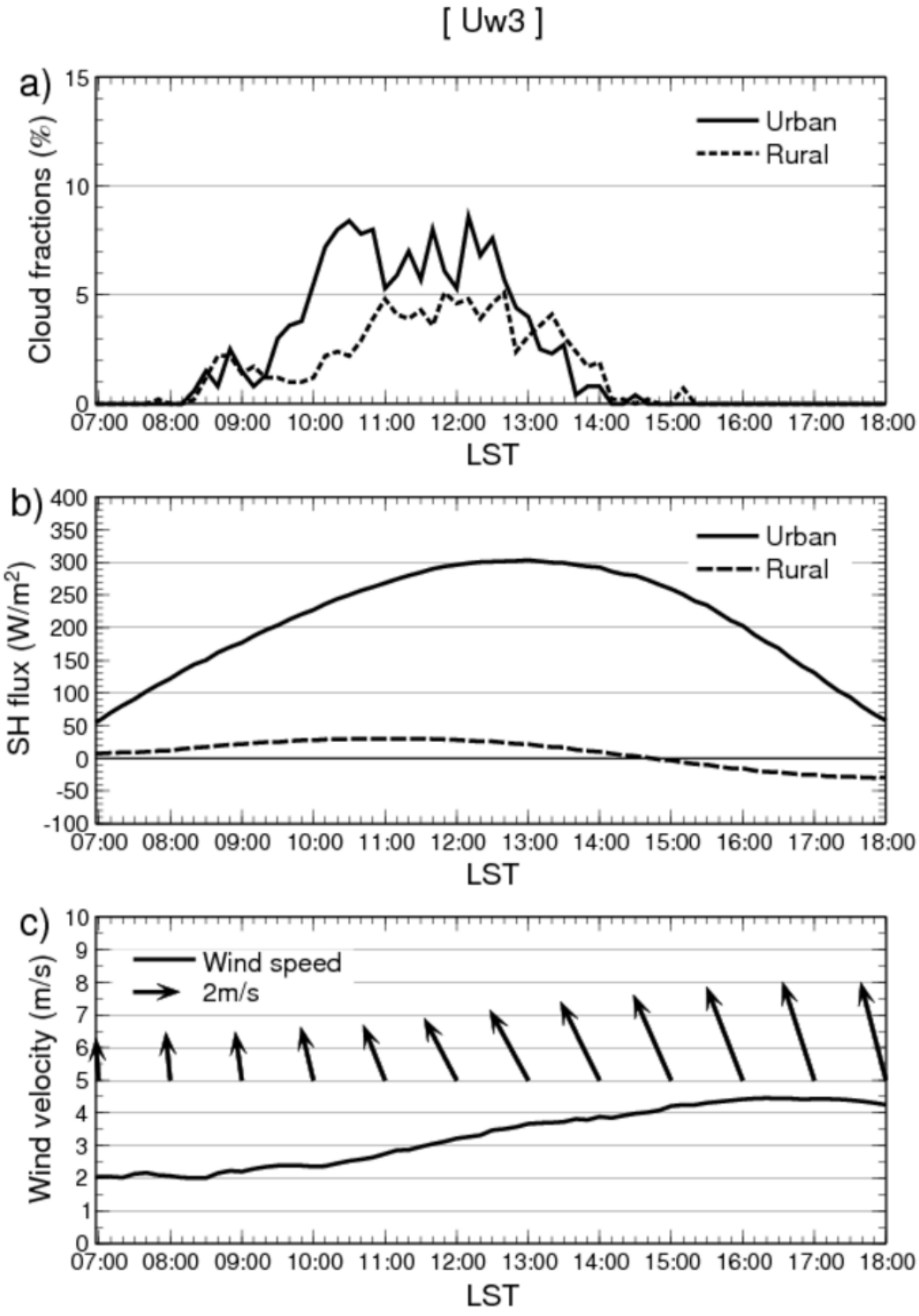

Figure 4.17: Same as Fig. 4.6 but for Case Uw3.

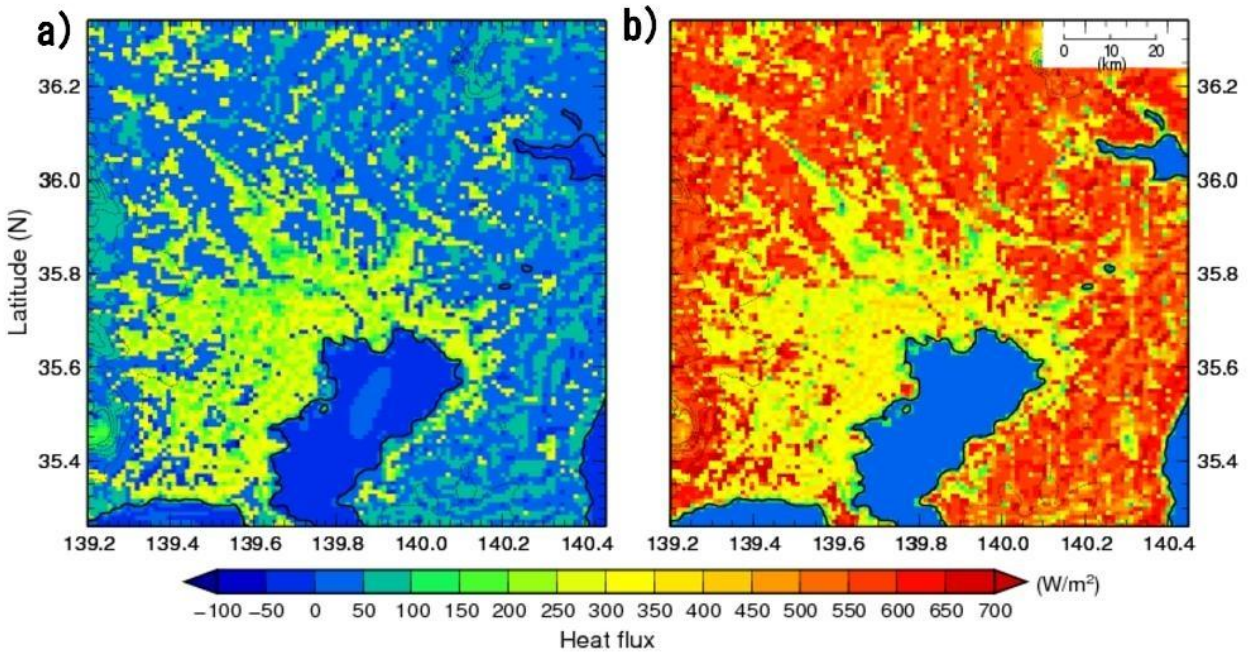

Figure 4.18: The horizontal distribution of (a) sensible heat flux and (b) latent heat flux at 1030 LST in CTRL.

Table 4.1: Lifetime of the cloud lines in each extending urban area (EUA).

EUA	Onset and dissipation time of line-shape clouds	Lifetime of line-shape clouds (hours)
a	1110 – 1140 LST	0.5
b	0850 – 1300 LST	4.2
c	0820 – 1110 LST	2.8

Table 4.2: Features of thermal sensitivity experiments.

	CTRL	U75	U85	N00
Onset time of urban cloud	0810 LST	0840 LST	0900 LST	0910 LST
Sensible heat flux at onset time (W/m^2) Urban / Rural	130 / 23	82 / 32	51 / 39	(42)
Cloud fraction	Urban >> Rural	Urban > Rural	Urban >= Rural	--
Index ratio of sensible heat flux	6.9	4.3	1.9	--
Maximum sensible heat flux (W/m^2) Urban / Rural	297 / 43	199 / 46	92 / 49	(49)
Time (LST)	1240 / 1110	1300 / 1110	1300 / 1110	(1130)
Urban cloud base height at 1100 LST	1271 m	1115 m	1012 m	(929 m)

5. Conclusions

The horizontal frequency distribution of shallow clouds is estimated around the Tokyo metropolitan area using NOAA satellite images obtained for summer days without regional-scale cloud cover during an 11-year period. The frequency of shallow clouds is higher over the urban area than rural areas in the early afternoon; in particular, cloud formation is reinforced over the radially extending urban areas along the major railroads from the metropolis. The distributions of NDVI and the frequency of low-level clouds correlate spatially well within a shift of only about 2 km. This implies that low-level clouds form at the top of the thermals in the mixed layer enhanced by a stronger sensible heat flux in the urban area. A stronger sensible heat flux over the urban area enhances the depth of the mixed layer. The frequency of the low-level clouds is low in the coastal urban zone located within about 10 km from the coastline. The bay and sea breezes seem to suppress the height of the mixed layer. The urban effects on cloud formation are weaker than those by the land-sea contrast and mountains.

To investigate the features of the urban clouds, the ground-based photographic observation of the urban clouds was conducted around Saitama City, where the difference of cloud frequency between urban and nearby rural areas is sharpest. The urban clouds were observed on 12 days in 54 days when photographs were taken. The horizontal cloud distribution was observed by MODIS images, and the urban clouds in the pictures were confirmed to form over the urban area. In most cases, onset time of the urban clouds was between 0800 LST and 1130 LST and dissipation time was between 1300 LST and 1700 LST, although the time evolution of clouds somewhat depended on days. The duration of the cloud forming ranged between 3 to 6 hours in most days. Those clouds were generally "active cumulus clouds". The clouds were gradually developed and became Cumulus congestus in the early afternoon on some of those days.

The observed small cumulus clouds formed above the urban areas along railroad lines are

simulated by the numerical model and elucidated its mechanisms. The distribution and the time evolution of those simulated clouds agree well with those of the satellite images and the ground-based photographic observation on typical days. The model indicates that the small clouds are not only enhanced in the urban areas but also suppressed in surrounding rural areas. The distribution of small clouds is sensitive to the thermal contrast between urban and rural. When the ratio of maximum sensible heat flux between urban and rural is about seven, the contrast between the cloud formation in the urban areas and the cloud suppression in the rural areas is very clear. The small clouds are formed only in the urban areas but very rare in rural areas, because urban effects on cloud suppression in rural areas are predominant. The contrast of cloud fraction between urban and rural gradually decreases with the reduction of the thermal contrast. The contrast of cloud fraction is weakened but is still clear when the ratio of maximum sensible heat flux is 4.3. When the ratio is 1.9, the cloud suppression in the rural areas disappears.

The mechanism of the contrastive cloud formation between urban and rural is as follows: 1) Thermals form in the mixed layer above the land surface. 2) Because of the larger sensible heat flux, the mixed layer tends to be higher in the urban area; thus, thermals reach the lifting condensation level more easily than they do in the rural area. 3) The wide compensating downdrafts of the strong urban thermals cover the entire rural area and suppress thermals and clouds there.

Acknowledgments

I am most grateful to Prof. Fujio Kimura for supporting my all research activities. I also thank Prof. Hiroyuki Kusaka and Dr. Tomonori Sato for many important advises and useful discussions. A lot of comments and suggestions are given from Prof. Hiroshi. L. Tanaka, Prof. Yousay Hayashi, Prof. Hiroaki Ueda, and Prof. Kenichi Ueno in University of Tsukuba. Appreciation extends to Mr. Masayuki Hara and Dr. Hiroaki Kawase of Frontier Research Center for Global Change and Ms. Sachiho Adachi in University of Tsukuba. Their advices and cooperation on the data processing and model operations were always very helpful to my studies. I want to thank Mr. Shinya Nakata and Mr. Yasuhiro Kiuchi for supporting the observation. I also thank Prof. Hiroyuki Iwasaki in Gunma University for lending the observation equipments. It was very thoughtful of Fujimi Fire Department, Saitama Central Fire Department, and some elementary schools and junior high schools in Saitama City in Saitama Prefecture for providing observation sites. I wish to express my thanks to the members of the meteorological and climatological group of University of Tsukuba. I thank Ms. Ryoko Fukao and Ms. Tomoe Higuchi for their assistance. Finally, I am grateful to my wife, Yoriko, for her encouragement and support.

This research was partially supported by the Ministry of Education, Science, Sports and Culture, Grant-in-Aid for Scientific Research Category B, 17310003 and by the Global Environment Research Fund (S-5-3) of the Ministry of the Environment, Japan and by the Sasakawa Scientific Research Grant from The Japan Science Society.

References

Avissar, R. and Y. Liu (1996), Three-dimensional numerical study of shallow convective clouds and precipitation induced by land surface forcing, *J. Geophy. Res.*, **101**, 7499-7518.

Baik, J.-J., Y.-H. Kim, and H.-Y.Chun HY (2001), Dry and moist convection forced by an urban heat island, *J. Appl. Meteor.*, **40**, 1462-1475.

Bornstein, R. and Q. Lin (2000), Urban heat islands and summertime convective thunderstorms in Atlanta: three case studies., *Atmos. Environ.*, **34**, 507-516.

Braham Jr., R. R.and D. Wilson (1978), Effects of St. Louis on convective cloud heights., *J. Appl. Meteor.*, **17**, 587-592.

Changnon Jr. S. A., F. A. Huff, and R. G. Semonin (1971), METROMEX: and investigation of inadvertent weather modification., *Bul. Amer. Moteor. Soc.*, **52**, 958-967.

Changnon Jr. S. A., R. G. Semonin, and F. A. Huff (1976), A Hypothesis for Urban Rainfall Anomalies., *J. Appl. Meteor.*, **15**, 544-560.

Changnon, S.A. (1978), Urban effects on severe local storms at St. Louis, *J. Appl. Meteor.*, **17**, 578-586. doi:10.1175/1520-0450(1978)017<0578:UEOSLS>2.0.CO;2

Chen, F. and R. Avissar (1994), Impact of land-surface moisture variability on local shallow convective cumulus and precipitation in large-scale models. *J. Appl. Meteor.*, **33**, 1382-1401.

Chen, S., and W. R. Cotton (1988), The sensitivity of a simulated extratropical mesoscale convective system to longwave radiation and ice-phase microphysics, *J. Atmos. Sci.*, **45**, 3897-3910.

Frisbie, P. R., and J. G. Hudson (1993), Urban cloud condensation nuclei spectral flux, *J. Appl. Meteor.*, **32**, 666-676.

Fujibe, F. and T. Asai (1980), Some features of a surface wind system associated with the Tokyo heat island., *J. Meteor. Soc. Japan*, **58**, 149-152.

Fujibe, F. (1998), Spatial anomalies and long-term changes of precipitation in Tokyo., *Tenki*, **45**, 7-18 (in Japanese with English abstract).

Fujibe, F. (2003), Long-term surface wind changes in the Tokyo metropolitan area in the afternoon of sunny days in the warm season., *J. Meteor. Soc. Japan*, **81**, 141-149.

Fujibe F. (2004) Effect of heat island to precipitation-convective precipitation in summer., *Tenki*, **51**, 109-115 (in Japanese).

Grosh, R. C. (1978), Satellite-observed urban cloud distributions, *Summary of METROMEX, Vol. 2: Causes of precipitation anomalies. Bull. 63*, Illinois State Water Survey, Urbana, 229-235.

Hildebrand, H. and B. Ackerman (1984), Urban Effects on the Convective Boundary Layer., *J. Atmos. Sci.*, **41**, 76-91.

Hjelmfelt, M. R. (1982), Numerical Simulation of the Effects of St. Louis on Mesoscale Boundary-Layer Airflow and Vertical Air Motion: Simulations of Urban vs Non-Urban Effects., *J. Appl. Meteor.*, **21**, 1239-1257.

Ichinose T., K. Shimodozono, and K. Hanaki (1999), Impact of anthropogenic heat on urban climate in Tokyo., *Atmos. Environ.*, **33**, 3897-3909.

Jin, M. L., J. M. Shepherd, and M. D. King (2005), Urban aerosols and their variations with clouds and rainfall: A case study for New York and Houston., *J. Geophy. Res.-Atmos.*, **110**., D10S20., doi:10.1029/2004JD005081.

Kanda M, Y. Takayanagi, H. Yokoyama and R. Moriwaki (1997), Field observation of the heat balance in an urban area., *J. Japan Soc. Hydrol. & Water Resour.*, **10**, 329-336 (in Japanese with English abstract).

Kanda M, Y. Inoue, and I. Uno (2001), Numerical study on cloud lines over an urban street in Tokyo, *Bound.-Layer Meteor.*, **98**, 251-273, doi:10.1023/A:1026504904902.

Kimura, F. and S. Takahashi (1991), The effects of land-use and anthropogenic heating on the surface temperature in the Tokyo metropolitan area: A numerical experiment., *Atmos.*

Environ. **25B**, 155 - 164.

Klemp J. B. and R. B. Wilhelmson (1978), The simulation of three-dimensional convective storm dynamics., *J. Atmos. Sci.*, **35**, 1070-1096.

Kusaka, H., F. Kimura, H. Hirakuchi, and M. Mizutori (2000), The effects of land-use alteration on the sea breeze and daytime heat island in the Tokyo metropolitan area., *J. Meteor. Soc. Japan*, **78**., 405-420.

Kusaka H., H. Kondo, Y. Kikegawa, and F. Kimura (2001), A simple single-layer urban canopy model for atmospheric models: Comparison with multi-layer and slab models, *Bound.-Layer Meteor.*, **101**, 329-358. doi:10.1023/A:1019207923078

Nakajima, T., M. Tsukamoto, Y. Tsushima, A. Numaguti, and T. Kimura (2000), Modeling of the radiative process in an atmospheric general circulation model, *Appl. Opt.*, **39**, 4869-4878.

Ochs, H.T. (1975), Modeling of Cumulus Initiation in METROMEX, *J. Appl. Meteor.*, **14**, 873-882, doi:10.1175/1520-0450(1975)014<0873:MOCIIM>2.0.CO;2.

Ochs, H. T., and R. G. Semonin (1979), Sensitivity of a cloud microphysical model to an urban environment, *J. Appl. Meteor.*, **18**, 1118-1129.

Pielke R. A., W. R. Cotton, R. L. Walko, C. J. Tremback, W. A. Lyons, L. D. Grasso, M. E. Nicholls, M. D. Moran, D. A. Wesley, T. J. Lee, and J. H. Copeland (1992), A comprehensive meteorological modeling system-RAMS., *Meteorol. Atmos. Phys.*, **49**, 69-91. doi:10.1007/BF01025401.

Rabin R. M. and D. W. Martin (1996), Satellite observations of shallow cumulus coverage over the central United States: An exploration of land use impact on cloud cover. *J. Geophys. Res.*, **101(D3)**, 7149-7155, doi:10.1029/95JD02891.

Romanov P. (1999), Urban influence on cloud cover estimated from satellite data, *Atmos. Environ.*, **33**, 4163-4172, doi:10.1016/S1352-2310(99)00159-4.

Rotach M. W., R. Vogt, C. Bernhofer, E. Batchvarova, A. Christen, A. Clappier, B. Feddersen, S.-E. Gryning, G. Martucci, H. Mayer, V. Mitev, T. R. Oke, E. Parlow, H. Richner, M. Roth,

Y.-A. Roulet, D. Ruffieux, J. A. Salmond, M. Schatzmann and J. A. Voogt (2005), BUBBLE - An urban boundary layer meteorology project., *Theor. Appl. Climatol.*, **81**, 231-261, doi:10.1007/s00704-004-0117-9.

Sato, N and M. Takahashi (2000), Long-term changes in the properties of summer precipitation in the Tokyo area., *Tenki*, **47**, 643-648 (in Japanese with English abstract).

Sato, T, T. Terashima, T. Inoue, and F. Kimura (2006), Intensification of convective precipitation systems over Tokyo urban area in summer season., *Tenki*, **53**., 479-484 (in Japanese with English abstract).

Shepherd, J. M., H. Pierce, and A. J. Negri (2002), Rainfall modification by major urban areas: Observations from spaceborne rain radar on the TRMM satellite., *J. Appl. Meteor.*, **41**., 689-701.

Shepherd, J. M. (2005), A Review of Current Investigations of Urban-Induced Rainfall and Recommendations for the Future., *Earth Interactions*, **9**, 1-27, doi:10.1175/EI156.1.

Shreffler J. H. (1978), Detection of centripetal heat-island circulations from tower data in St. Louis., *Bound.-Layer Meteor.*, **15**, 229-242, doi:10.1007/BF00121924.

Stull, R.B. (1985), A Fair-Weather Cumulus Cloud Classification Scheme for Mixed-Layer Studies, *J. Appl. Meteor.*, **24**, 49-56.

Stull R.B. (1988), *An introduction to boundary layer meteorology*, 666 pp., Kluwer Academic Pablishers.

Tripoli, G. J., and W. R. Cotton (1980), A numerical investigation of several factors contributing to the onserved variable intensity of deep convection over South Florida., *J. Appl. Meteor*., **19**, 1037-1063.

Yonetani, T (1982), Increase in number of days with heavy precipitation in Tokyo urban area, *J. Appl. Meteor*., **21**, 1466-1471.

Yoshikado H. and H. Kondo (1989), Inland penetration of the sea breeze over the suburban area of Tokyo,., *Bound.-Layer Meteor.*, **48**, 389-407

Yoshikado H (1990), Vertical structure of the sea breeze penetrating through a large urban complex., *J. Appl. Meteor*., **29**, 878-891.

Zhu, P. and B. Albrecht (2003), Large eddy simulations of continental shallow cumulus convection, *J. Gephys. Res.*, **108**, 4453, doi:10.1029/2002JD003119.